Towards bone graft manufacturing via endochondral ossification

Inauguraldissertation

zur
Erlangung der Würde eines Doktors der Philosophie
vorgelegt der
Philosophisch-Naturwissenschaftlichen Fakultät
der Universität Basel

von

Beatrice Tonnarelli

aus **Italien**

Basel, 2012

creative commons

Attribution-Noncommercial-No Derivative Works 2.5 Switzerland

---

You are free:

to Share — to copy, distribute and transmit the work

Under the following conditions:

Attribution. You must attribute the work in the manner specified by the author or licensor (but not in any way that suggests that they endorse you or your use of the work).

Noncommercial. You may not use this work for commercial purposes.

No Derivative Works. You may not alter, transform, or build upon this work.

- For any reuse or distribution, you must make clear to others the license terms of this work. The best way to do this is with a link to this web page.
- Any of the above conditions can be waived if you get permission from the copyright holder.
- Nothing in this license impairs or restricts the author's moral rights.

Your fair dealing and other rights are in no way affected by the above.

This is a human-readable summary of the Legal Code (the full license) available in German:
http://creativecommons.org/licenses/by-nc-nd/2.5/ch/legalcode.de

Disclaimer:
The Commons Deed is not a license. It is simply a handy reference for understanding the Legal Code (the full license) — it is a human-readable expression of some of its key terms. Think of it as the user-friendly interface to the Legal Code beneath. This Deed itself has no legal value, and its contents do not appear in the actual license. Creative Commons is not a law firm and does not provide legal services. Distributing of, displaying of, or linking to this Commons Deed does not create an attorney-client relationship.

Quelle: http://creativecommons.org/licenses/by-nc-nd/2.5/ch/deed.en Datum: 3.4.2009

Genehmigt von der Philosophisch-Naturwissenschaftlichen Fakultät

auf Antrag von

Prof. Ueli Aebi Prof. Dr. Giuseppe Peretti Prof. Ivan Martin

Basel, den 21/06/2011

Prof. Dr. Martin Spiess

Basel, June 6th 2011

alla mitica bici benotto

le reve, c'est tout -

la technique, ca s'apprend.

jean tinguely

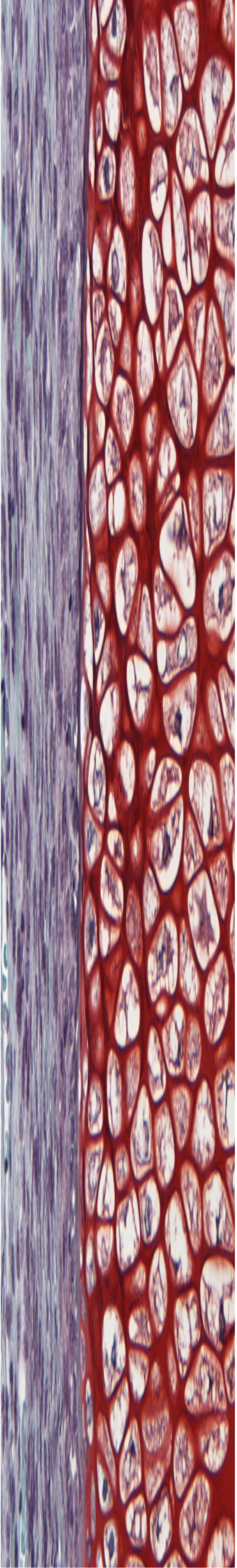

Table of Contents

Introduction

1. Long bone and articular cartilage development

Skeletal structures in the body withstand load bearing, allow adjacent muscles to move them in coordination with specialized joint structures, protect adjacent organs, and serve as mineral reservoir that can be mobilized on metabolic demand.

Location and type of bone and articular cartilage structures in the body select their initial development and ultimate function. Sizes and shapes of bones need to be carefully controlled and tuned to exert specific functions in efficient manner and in specific environments. Therefore bone is a dynamic tissue with a unique capacity to remodel.

On the contrary, cartilage of the skeletal system is a quiescent connective tissue with poor remodeling activity but important load bearing and motility functions.

Hormone/growth factor signaling pathways tightly coordinate both skeletal development and remodeling, throughout the individual lifespan. Among several paracrine morphogens, bone morphogenetic proteins (BMPs), Wnts, fibroblast growth factors (FGFs) and hedgehog proteins are essential for normal bone formation. Moreover, systemic factors such as growth hormone, thyroid hormone, oestrogen, androgen, vitamin D and glucocorticoids contribute to control skeletal growth (Kronenberg 2003).

During embryogenesis, skeletal formation begins when cells from mesenchyme start to condense (Hall and Miyake 2000).

For all bones of axial system, cartilage is the first skeletal tissue to be formed by mesenchymal progenitors and subsequently remodeled into bone through a program called endochondral route (Figure 1a).

On the contrary, flat bones such as skull develop via direct differentiation of condensed mesenchymal cells into bone forming osteoblasts bypassing cartilaginous intermediate and undergoing membranous or intramembranous ossification (Quintana, zur Nieden and Semino 2009) (Figure 1b).

The two developmental processes differ from (i) location and type of skeletal elements where they occur (flat or long bones), (ii) key morphogenetic pathways involved, (iii) intermediate and terminal cell differentiation stages and (iv) extracellular matrix (ECM) composition. These structural and functional differences are crucial aspects for repair processes and regenerative medicine approaches.

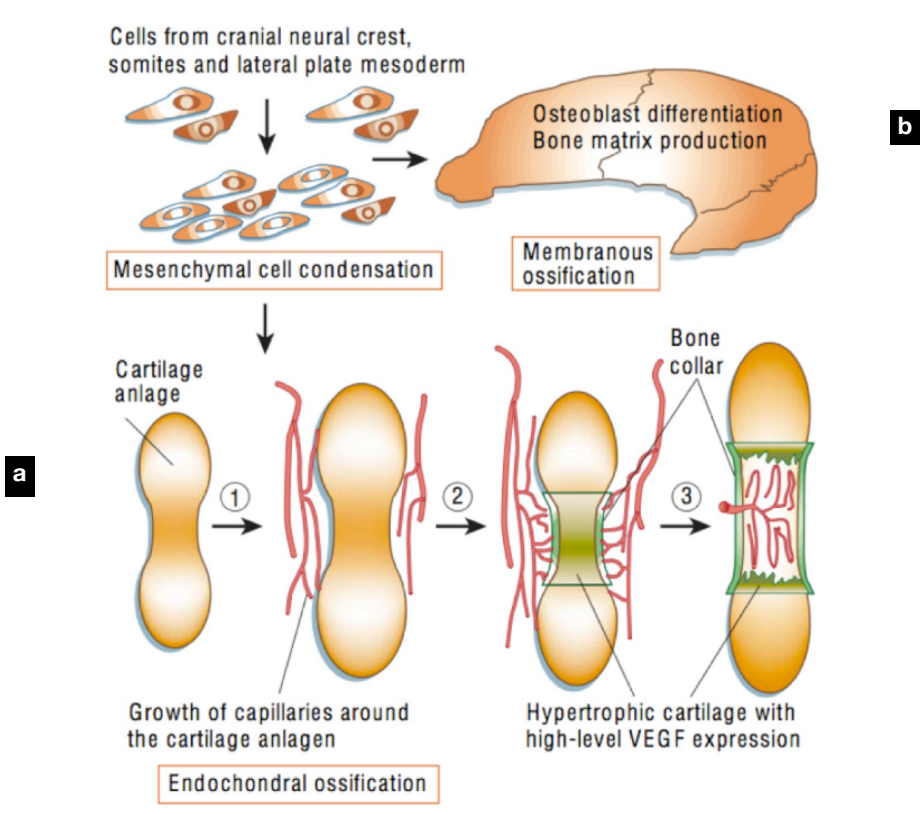

Figure 1 *Mesenchymal cells condense at sites of future bones. In endochondral ossification route (a), first a cartilage model (anlage) is formed; this tissue undergoes hyperthrophy while a collar of bone appears at the periphery and vessels ingrowth begins, thanks to the developing gradients of angiogenic factors such as vascular endothelial growth factor (VEGF); finally, hyperthrophic cartlage is replaced by marrow and bone and growth plates are formed. In membranous ossification process (b), direct differentiation of mesenchymal cells to osteoblasts and production of bone matrix occurs (adapted from Zelzer and Olsen 2003).*

1.1 Endochondral bone formation

Long bone and axial skeleton formation occurs through a process called endochondral ossification, as a result of coordinated cell migration, proliferation, differentiation, and remodeling of cartilaginous matrix templates. In the developing limb, early bone formation begins with migration of undifferentiated mesenchymal cells from the mesoderm to the limb bud following morphogenetic signals made by apical ectodermal region (Sundelacruz and Kaplan 2009).

Rapidly proliferating mesenchymal cells that have been recruited into the bone-forming region commit to chondrogenic lineage, aggregate to form compact nodules, and secrete extra cellular matrix (ECM) firstly enriched in collagen type I and hyaluronan (ten Berge, et al. 2008) (Figure 2).

This condensation phase is associated with a decrease in extracellular space and involves changes in cell–cell and cell–matrix interactions, which are mediated by adhesion molecules including N-cadherin and fibronectin. Condensed cells keep on proliferating and differentiating to form a soft callus (cartilage anlage) that provides mechanical support while acting as a template for future bone deposition. Chondrocyte differentiation is characterized by synthesis of cartilage-supporting matrix, including collagens II, IX, and XI, and aggrecan and other proteoglycans (Figure 2).

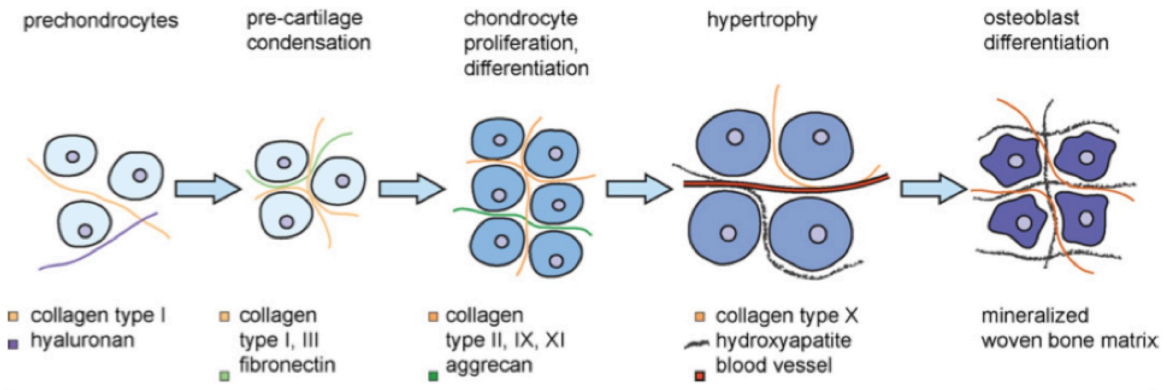

Figure 2 Extra cellular matrix (ECM) changes during endochondral ossification. Cells produce and remodel the matrix, which, in turn, provides physical and biochemical stimuli to the cells (adapted from Sundelacruz and Kaplan 2009).

Chondrocytes mature further, and undergo hypertrophy. The composition of the ECM changes due to chondrocyte secretion of collagen type X and matrix metalloprotease 13 (MMP13) (Figure 2). Late differentiated chondrocytes positioned in the centre of the cartilaginous mould ultimately stop proliferating and become apoptotic. On the contrary, the ones in closed proximity with the external part, the perichondrium, undergo a different fate and perform multiple tasks as they are exposed to unique matrix components and cellular crosstalks. Upon transitional chondrogenic activity, these latter cells are prompted to differentiate towards the osteogenic lineage actively contributing to bone formation as they mineralize the ECM by producing bone sialo-protein (BSP) and depositing hydroxyapatite. Thanks to the localization and dual differentiation potential, they have been named “borderline” chondrocytes and they contribute to the formation of the external bone collar (Figure 3).

Interestingly, chondrocytes contribute to tissue formation and to tissue removal, respectively at bony collar and growth plate (Bianco, et al. 1998). Even if cartilage itself is characterized by its avascular nature, terminal hypertrophic chondrocytes become actually a target for vascular invasion by expressing high levels of angiogenic molecules, such as vascular endothelial growth factor (VEGF). Thus, capillaries first grow around the cartilage anlage and then invade the remodeled matrix by crossing the developing bone collar. Initial blood vessel invasion of the cartilaginous bone model occurs in parallel with its transformation into the primary OSSIFICATION center (POC) (Figure 3). ECM degradation and angiogenic gradients allow for vascular invasion and recruitment of osteoblastic, osteoclastic, and hematopoietic precursors from peripheral blood stream. Early osteoblasts precursors, characterized by the expression of the primitive marker Osterix and in closed association with pericytes, translocate into the developing POC and contribute to the stroma or produce trabecular bone. The first committed osteoblast lineage cells localize in the perichondrium surrounding the hypertrophic cartilage whereas mature osteblastic cells (expressing collagen type I) are present in the cortical bone surfaces. As well as chondrocytes, osteoblastic cells display differential destinies depending on their stage of maturation and location (Maes et al. 2010) (Figure 4).

The osteoclasts, bone remodeling cells, degrade most of the matrix surrounding hypertrophic chondrocytes

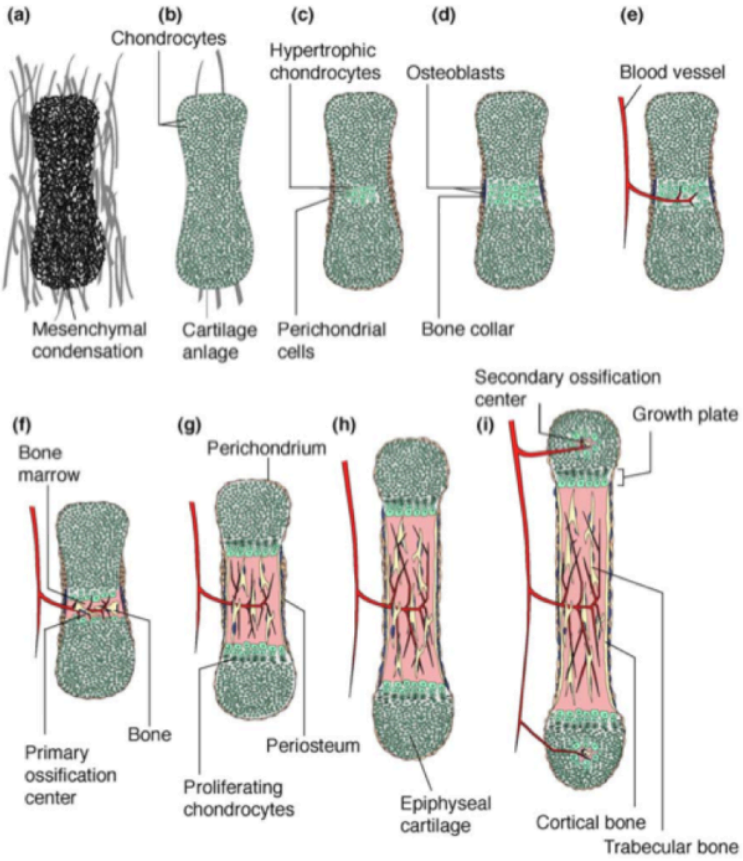

Figure 3 *"Endochondral bone development. (a, b) Chondrocytes differentiate within mesenchymal condensations to form cartilage anlagen of future bones. (c, d) Coincident with the appearance of the perichondrial bone collar, chondrocytes in the central anlage undergo hypertrophy followed by invasion of vascular and osteoblastic cells from the collar (e) and formation of the primary ossification center (f). This process expands toward the ends of the bone, eventually forming mature growth plates (h). Secondary ossification centers later form in the epiphyseal cartilage (i)." (from Horton and Degnin 2009)*

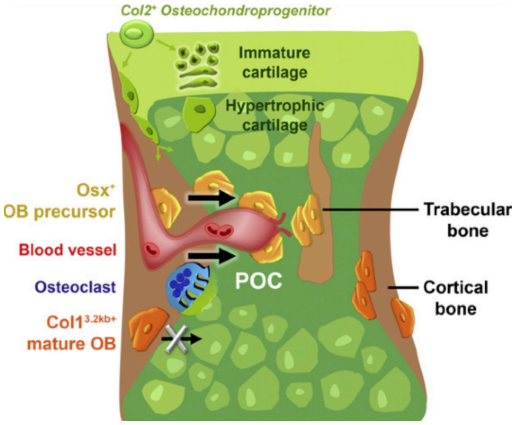

Figure 4 *"Schematic outline of the events taking place during the initial invasion of the cartilaginous bone model and its transformation into the primary ossification center (POC). Chondro-perichondrial progenitors (Col2+, green) give rise to cells in the central growth cartilage. The first committed osteoblast lineage cells appear in the perichondrium surrounding the middiaphyseal hypertrophic cartilage. Early cells of the lineage, represented by the Osx-expressing osteoblast precursors (Osx+, yellow), move into the developing POC and populate it as stromal cells or differentiate further to become bone-forming trabecular osteoblasts. The entrance of the osteoblast precursors into the POC coincides with the initial invasion by blood vessels (red) and osteoclasts (blue), and is associated with a pericytic localization of a subset of the precursors onto the endothelium. In contrast, differentiated cells within the perichondrium/periosteum (Col1+ mature osteoblasts, orange) are not found in vessel-covering positions and do not have the capacity to translocate into the POC. These osteoblasts are retained on and within the cortical bone surfaces" (from Maes et al. 2010)*

leaving fragments that serve as scaffolding for deposition of bone matrix by the osteoblasts. As the bone enlarges, haematopoietic stem cells interact with the stroma and become established in spaces between the bony trabeculae creating the main site for haematopoiesis in post-natal life (Figure 3).

At this stage of the endochondral route, hypertrophic cartilage is replaced by marrow and bone, along with vascular invasion, and in forming long bony parts epiphyses and metaphyses at each end and diaphysis in between are established (Figure 3).

The epiphyses play a key role in determining the transverse and spherical growth of the ends of the bone, the shaping of the articular surfaces, and the longitudinal growth of the metaphyses and the diaphysis. Growth plates are finally formed at the interface between metaphysis and epiphysis (Figure 5) (Shapiro 2008).

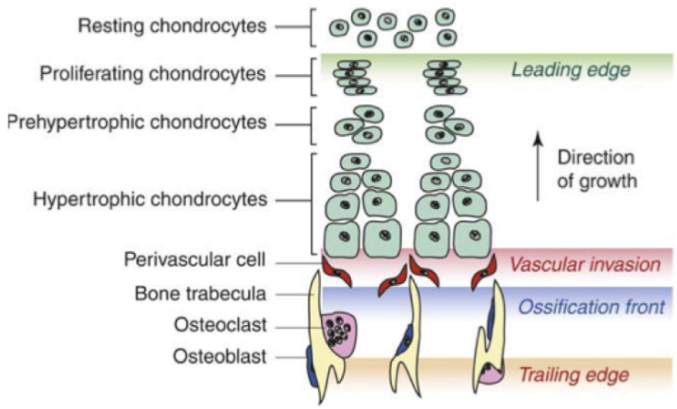

Figure 5 *"Growth plate structure. The growth plate is dynamic with a leading edge (green) where chondrocytes proliferate and a trailing edge (brown) where cartilage template generated by the proliferating and terminally differentiating chondrocytes is degraded by invading vascular cells (red) and replaced by the expanding ossification front (blue)" (from Horton and Degnin 2009)*

A portion of chondrocytes (columnar chondrocytes) in the centre of the developing bone assumes a flattened, discoid shape and form columns oriented along the axis of bone lengthening, a process they control primarily by the rate of differentiation into hypertrophic chondrocytes.

The soft transient cartilaginous callus has been gradually replaced by hard woven bone, with the exception for articular cartilage that is stable at the joint site (Kronenberg 2003). As a matter of fact, each epiphysis develops into: i) cartilage adjacent to the joint space, the articular cartilage, characterized by quiescent chondrocyte cell population and collagen type II rich matrix ii) cartilage adjacent to the metaphysis, the growth plate, and iii) cartilage between the articular cartilage and the physeal cartilage, the epiphyseal cartilage, which will form a secondary ossification center upon invasion by vessels and osteoprogenitors (Shapiro 2008). This anatomical distinction exemplifies the development of two different kinds of cartilage by MSCs: (1) persistent and stable cartilage at the joint site and (2) transient cartilaginous models elsewhere that will accomplish endochondral ossification (Pelttari, Steck, and Richter 2008).

As bones enlarge further, so-called secondary ossification centers are established, in the epiphyses of the newly formed bone by the same processes occurring for the first ossification centre. Growth plate chondrocytes continue to proliferate between regions of bone of the primary and secondary ossification centers to allow bone elongation, a process that will stop at time of adolescence.

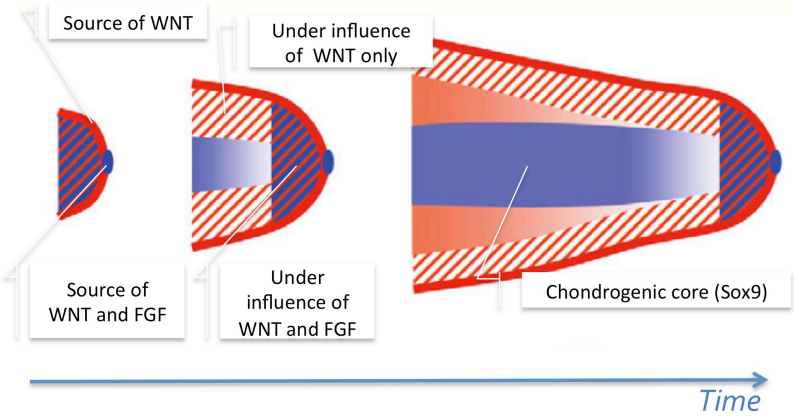

Figure 6 "Wnt and FGF signals interact to coordinate growth and cell fate specification during limb development. In the newly established limb bud, both Wnt and FGF proteins signal throughout the limb mesenchyme and maintain all cells in a multipotent, proliferative state (region indicated by red/blue hatching). Following limb outgrowth, cells in the center of the limb are no longer within range of the signals. This allows cell cycle withdrawal and expression of Sox9, leading to establishment of the chondrogenic core (indicated in blue)" (adapted figure and caption from ten Berge et al. 2008).

1.2 Focusing on molecular pathways

Endochodral bone formation is influenced by morphogen crosstalks among different cell types. The list of signalling factors affecting growth plate development is long and not fully characterized from the molecular stand point. Cytokines, growth hormone, retinoids, thyroid hormone, oestrogen, androgen, vitamin D and glucocorticoids among others, exert important roles during embriological development and postnatal remodelling (Kronenberg 2003).

In the developing limb bud, the influence of FGF and Wnt signals from the surrounding tissue firstly maintains mesenchymal cells in an undifferentiated proliferative state and thus coordinates tissue growth and cell fate determination (Ten Berge et al 2008; Figure 6).

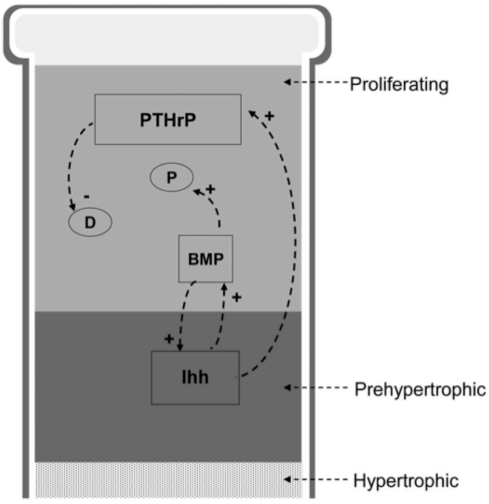

Figure 7 "Interactions between proliferating and prehypertrophic chondrocytes in the growth plate. In response to Ihh signaling, PTHrP is secreted by the proliferating chondrocytes, reaches the prehypertrophic chondrocytes, and retards their progression to the hypertrophic state, thereby delaying column elongation and synchronizing it with cell differentiation and other processes taking place in parallel, such as secretion and organization of the extracellular matrix, which is needed for columnar structural integrity. In addition, Ihh regulates the expression of BMP genes, which also upregulate chondrocyte proliferation. BMP, bone morphogenetic protein; P, proliferation; D, differentiation" (from Lenas, Moos and Luyten 2009).

At condensation stage, progenitors are at least bipotential with regard to their final cell fate determination (Day and Yang 2008). Infact, during intra-membranous ossification, Wnt signaling is high and inhibits chondrocyte differentiation while promoting osteoblast differentiation. On the contrary, in endochondral ossification, Wnt signaling is kept low such that only chondrocytes can differentiate; similarly, Wnt signaling will be upregulated at the perichondrium where osteoblasts will differentiate. Upregulation of SOX9, SRY (sex determining region Y)-box 9, the main gene driving chondrocyte differentiation, occurs when cells in the center of the limb are no longer within the range of FGF and Wnt signals: the diminishing of the influence of the morphogens reflects the establishment of the chondrogenic condensed core (Horton and Degnin 2009). Cellular communication at this stage gets more complicated by the expression of further molecules such as Sonic Hedgehog (SHH) and BMP2 that play as important regulators of limb outgrowth.

Once the growth plate is established, maturing chondrocytes produce the signaling factor Indian Hedgehog (Ihh), a soluble molecule of the Hh family which exerts important roles in regulating proliferation, maturation rates, and ossification processes. Ihh promotes the expression of BMPs that, in turn, contribute to cartilage and bone formation by (i) upregulating chondrocyte proliferation, (ii) increasing the length of proliferating columns of chondrocytes and (iii) converting perichondral cells into osteoblasts.

Overall, BMPs antagonize the effects of FGF signalling (namely, shortening proliferative columns both by decreasing chondrocyte proliferation directly and by suppressing Ihh expression) at the site of proliferative (P) and terminal differentiated (D) chondrocytes (Figure 7) (Lenas, Moos, and Luyten 2009; Kronenberg 2003).

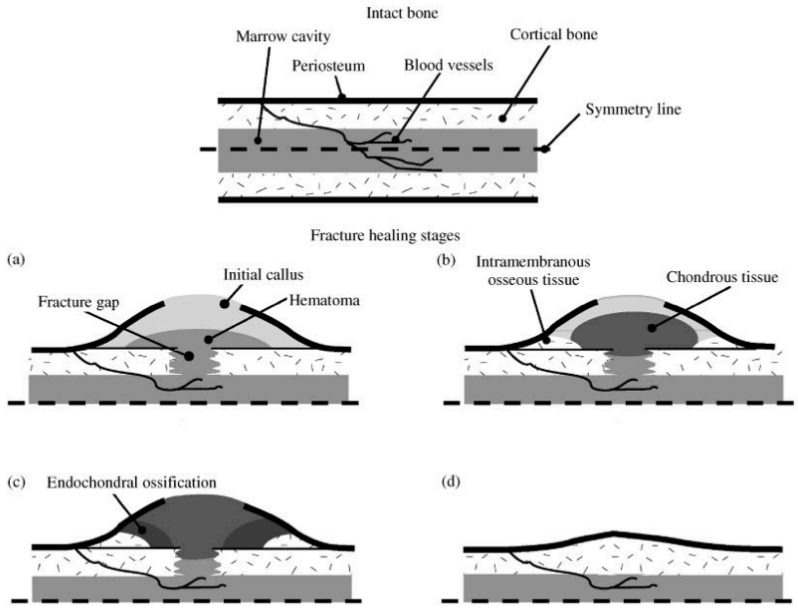

Figure 8 *Schematic of a section through an intact long bone and fracture healing stages. (a) inflammation: hematoma formation at the fracture gap and development of initial callus formed by mesenchymal cells; (b) callus differentiation: formation of chondrous tissue adjacent to the fracture and intramembranous ossification adjacent to the bone and distal to the fracture; (c) ossification: replacement of cartilaginous callus by osseous tissue via endochondral ossification, and (d) remodeling: restoration of original bone geometry (from Bailon-plaza and Van Der Meulen 2001)*

Interestingly, Ihh and BMPs seem to be essential at the point of divergence between persistent cartilaginous tissues (Meckel's cartilage of the mandible, nasal, ear, and intervertebral cartilages) and replacement ones that continue along the endochondral route in appendicular and axial skeleton. If chondrocytes lack expression of the pre-hyperthrophic markers (Ihh and BMP6), they fail to undergo hyperthrophy and consequently endochondral differentiation (Eames, de la Fuente and Helms 2003; Day and Yang 2008).

Moreover, in response to Ihh signaling, Parathormone (PTHrP) is secreted by proliferating chondrocytes at the end of the growth plate and by perichondral cells. This paracrine factor is a key player in the dialogue between cartilage and perichondrium. It primarily acts to maintain the proliferative pool of chondrocytes by feedback loop interplay with Ihh and it delays hyperthropy in prehypertrophic chondrocytes, in order to synchronize it with cell differentiation and ECM secretion and organization (Kronenberg 2003; Lenas, Moos, and Luyten 2009 part II) (Figure 7). The aforementioned signaling pathways interact in a spatio-temporally coordinated fashion and are fundamental regulators for limb development.

2. Repair capacity of skeletal tissue

2.1 …at the bone side…

Unlike other adult tissues, bone skeleton possess a unique capacity to heal after fracture, loss or damage by forming new bony tissue that is undistinguishable from adjacent injured parts and without leaving a scar.

This innate reparative and regenerative capacity of bone shares many features with development (Sundelacruz and Kaplan 2009). For example in both processes, 1) condensation and differentiation into cartilage-bone tissues occur with fetal and adult skeletal progenitors, 2) molecular markers of chondrogenesis and osteogenesis that regulate cell differentiation are conserved, 3) ECM remodeling and vascular invasion are strongly required (Colnot et al. 2003). Moreover, injured skeletal elements use cells of their own embryonic origin for repair (Leutch, et al. 2008; Gerstenfeld, et al. 2003). In case of bone fracture, structural and functional features must be re-established by creating morphogenetic fields and instructive cross talks between adjacent tissues, in analogy with specific bone development paths. Obviously, remarkable differences between development and repair process can be also identified: for instance mechanical forces and inflammation play important role in the latter, whereas they are not involved during development (Figure 8).

For example, after a fracture is sustained in a long bone structure, inflammatory response takes place with recruitment of macrophages and polymorphonuclear cells: an initial hematoma (Figure 8a) is formed under the control of several inflammatory factors. Soft callus with granulation tissue develops thanks to proliferative fibroblastic cells. When BMPs start to be produced, osteoprogenitors are induced to differentiate firstly into chondrocytes and then into osteoblasts following the endochondral route. Intramembranous ossification occurs only adjacent to reminiscent bony structures and distal to the fracture (Figure 8 b-c-d)

Therefore, molecular and cellular insights concerning intramembranous and endochondral bone formation not only offer deeper knowledge in developmental system biology but also contribute in understanding spontaneous healing processes of damaged or diseased bone and, thus, may also inform bioengineering strategies (Zelzer and Olsen 2003).

2.2 …at the cartilage side…

When a degenerative or traumatic injury occurs at the site of articular cartilage, unlikely what happens in bone lesions, the innate reparative capacity results in suboptimal and inefficient tissue recovery.

The avascular nature of the cartilage remarkably impairs the healing process because of the delay in recruitment of progenitors.

Nevertheless, the skeletal system tempts to reply to the injury by stimulating mesenchymal progenitor cells from the underlying subchondral bone and by relying on their capacity to undergo chondrogenic differentiation. This potential, unfortunately, can turn into a limitation: MSC-derived chondrocytes undergo premature hypertrophy and develop into a transient, endochondral cartilage, instead of stable, articular cartilage-like

tissue in line with the developmental endochondral pathway they recapitulate.
Thus, repair of articular defects with stable reparative tissue represents an open clinical challenge.

3. Skeletal defects: reparative and regenerative clinical strategies

In case of critically sized skeletal defects caused by post-traumatic tissue loss, benign or malignant tumors, atrophic nonunions, periprosthetic bone loss, arthrodesis, and degenerative diseases, spontaneous healing can not support tissutal and functional recovery. In the following paragraphs, an overview of current surgical procedures will be given. Moreover, tissue engineering and cell-based therapy concepts will be described as interesting alternatives to these conventional clinical approaches for skeletal regeneration.

3.1 Conventional techniques

3.1.1 ...for bone defects...

Skeletal defects requiring bone-graft repair procedures are estimated in 1 million clinical cases a year. Worldwide, socioeconomic consequences of such treatments represent a major concern, and will increase in the next years due the aging of their population. Current surgical procedures consist in autologous bone grafts, autogenous bone grafts or metallic and ceramic implants (Salgado, et al. 2004).
Autologous bone graft, that is bone taken from another site of the patient's own body, has been the gold standard of bone replacement for many years because it provides osteogenic cells as well as essential osteoinductive factors needed for bone healing and regeneration. Usually trabecular bone from the patient's iliac crest is taken, but cortical bone can be used as well. HIgh percentages of success are reached but limited amount of the autograft that can be obtained due to donor site morbidity.
Allograft, bone taken from somebody else's body, could be an alternative. However, the engraftment has lower chances than with the autograft due to immune rejections and pathogen transmission, that might be introduced.
As an alternative to these two bone grafts, there are metallic and ceramic prostheses to be implanted at the defect site. Metals, although providing immediate mechanical support at the site of the defect, exhibit corrosion, poor overall integration with the tissue at the implantation site, and may lead to surrounding bone resorption. Ceramics (e.g. bioglasses and calcium phosphates), on the other hand, show osteoconductivity and osteoinductivity but are brittle and not degradable (Salgado, et al. 2004).

3.1.2 ...for cartilage defects...

For chondral or osteochondral lesions, the ultimate clinical strategy is total replacement of the joint with me-

tallic prostheses. Nevertheless, according to the severity and the extension of the defects, some alternative treatment options can be taken into account. Marrow-stimulating techniques (e.g., microfracture or subchondral drilling of the bone) recall the principle of inducing invasion of mesenchymal progenitor cells from the underlying subchondral bone and promote the initiation of cartilage repair by chondrogenic differentiation of MSC. Unfortunately, the outcome of these procedures is highly variable and often results in fibrocartilaginous repair tissue, with limitations in quality and function as compared to native hyaline tissue. Mosaicplasty techniques exploit the possibility to harvest punches of autologous cartilage from non-bearing areas and to re-implant them in the damaged site. Obviously, also in this case, donor site morbidity and inferior repair tissue limit the clinical outcome (Pelttari, Steck, and Richter 2008).

3.2 Tissue engineering approach

In the last decades, new options in the field of regenerative medicine have been achieved thanks to the ability in tailoring and controlling in vitro fabrication of living replacement devices to ultimately restore in vivo tissue function (Vacanti and Langer 1993).
Researchers have been reaching this goal by combining the knowledge from physics, chemistry, engineering, materials science, biology, and medicine in an integrated manner, enclosed in the concept of Tissue

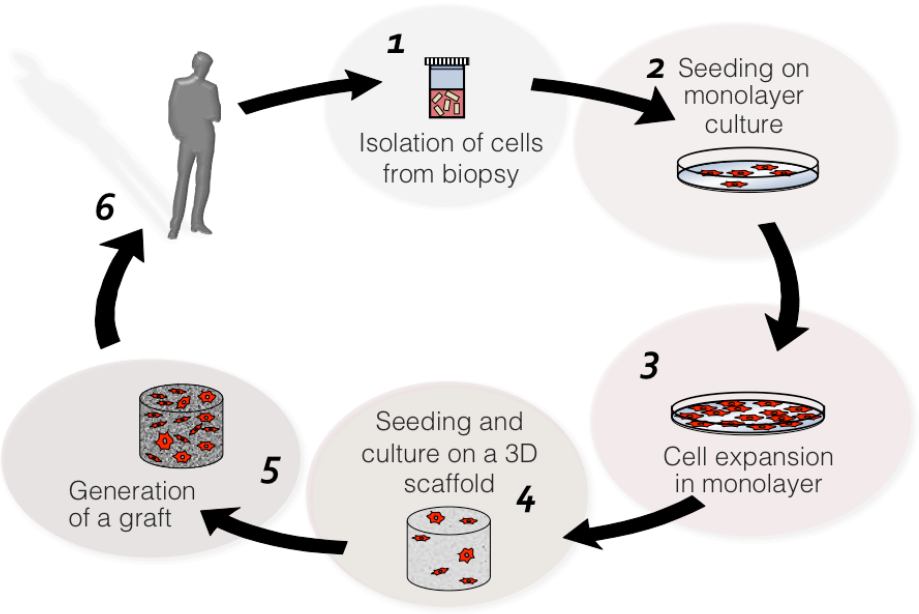

Figure 9 Schematic of conventional Tissue Engineering paradigm: 1) harvesting of tissue biopsy and isolation of regenerative cells; 2) cell seeding on monolayer surfaces (e.g. petri dishes, flasks); 3) cell expansion in monolayer till sufficient cell number is reached; 4) cell seeding into 3D scaffolds and maturation of the construct (cells and scaffold) in vitro; 5) complete generation of the graft and (6) implantation into the defect site

Engineering. Cells, scaffold and differentiating signals are the three key players for tissue engineering application and, although they could work individually, their combination might be beneficial for clinical applications.

Thus, nowadays, clinically relevant pre-formed tissue replacements, as well as ex-vivo human tissues serving as model systems, could be engineered (Sundelacruz and Kaplan 2009).

Ex vivo skeletal tissue manufacturing usually begins with cell harvesting from donor biopsy. Cells of interest are isolated (Figure 9 - step 1), usually plated in conventional monolayer expansion system (i.e. plates, flasks) (Figure 9 - step 2), and expanded until sufficient cell number is reached (Figure 9 - step 3). Then cells are collected and seeded either by gravity or by dynamic methods (e.g. centrifugation, spinner flasks, perfusion bioreactors) throughout 3D biomaterials (Figure 9 - step 4), that play as (i) cell carriers (ii) mechanical supports and (iii) informative biological cues. The graft generated could be further developed in vitro or directly re-implanted in vivo (Figure 9-steps 5 and 6).

Notably, as far as cell source is concerned, both developmental and regenerative skeletal formation processes are mediated by mesenchymal stem and progenitor cells.

Adult mesenchymal stem cells (MSC) have become the main source of choice for skeletal tissue engineering approaches as they meet several requirements for clinical applications such as (i) lower site morbidity for harvesting, (ii) good numerical yield upon in vitro expansion culture, (iii) broader differentiation capacity in comparison with differentiated primary cells (i.e. chondrocytes and osteoblasts).

Embryonic stem cells (ESCs) and the more recently developed iPS cells (induced pluripotent stem cells) are the most appealing cell source in terms of pluripotency. However, many factors have limited their application to human cell therapy, including ethical concerns, immunological incompatibilities, safety issue, potential for malignant tumor growth, heterogeneous differentiation, and an insufficient understanding and control of differentiation. For these reasons, adult MSCs are more clinically compliant for the current medical applications: MSC have the ability to generate skeletal tissue in a variety of experimental models, and hold great potential in cell based approaches for regenerative medicine (Sundelacruz and Kaplan 2009).

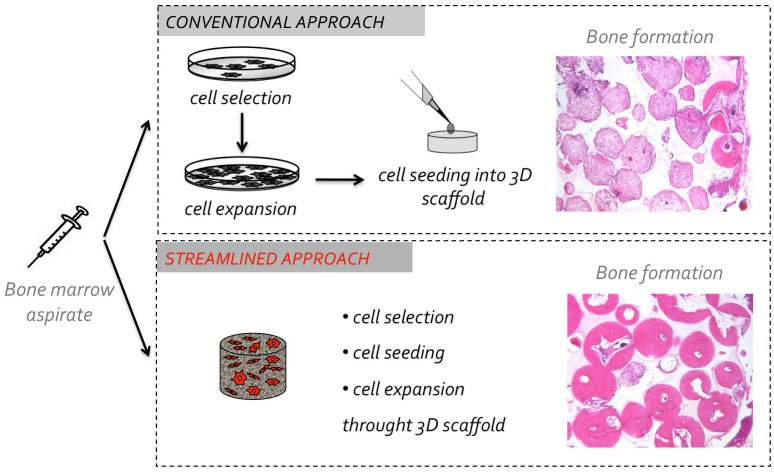

Figure 10 *Bone tissue engineering : example of implementation of conventional paradigm by performing cell selection, cell seeding and cell expansion directly throughout 3D scaffolds (results taken from Braccini et al. 2005)*

3.2.1 Bone tissue engineering

In the context of bone tissue engineering, thus far human adult MSC (e.g from bone marrow or adipose tissue) have been shown to generate bone exclusively through direct osteogenic differentiation (i.e., in a manner akin to intramembranous ossification), using a mineralized surface as “priming” substrate and, possibly, a boost of differentiating growth factors such as BMP2 (Axelrad and Einhorn 2009).

Different attempts in introducing novel paradigms have been made: it has previously been shown that adult MSC derived from bone marrow aspirate (Braccini, et al. 2005) (Figure 11) or lipoaspirate (Scherberich, et al. 2007) can be extensively expanded by loading and culturing freshly isolated cells directly within the pores of a 3D scaffold, ultimately generating an engineered construct in a simple streamlined process which completely bypasses the phase of monolayer expansion.

Despite encouraging in vitro results and few first clinical trials, the cost-benefit and the efficacy of bone tissue engineering approaches have still to be demonstrated. In fact, cell survival upon graft implantation still remains an unsolved issue, mainly for the lack of efficient coupling between vasculogenic and osteogenic potential, and thus, impairs the clinical outcome of tissue engineering approach.

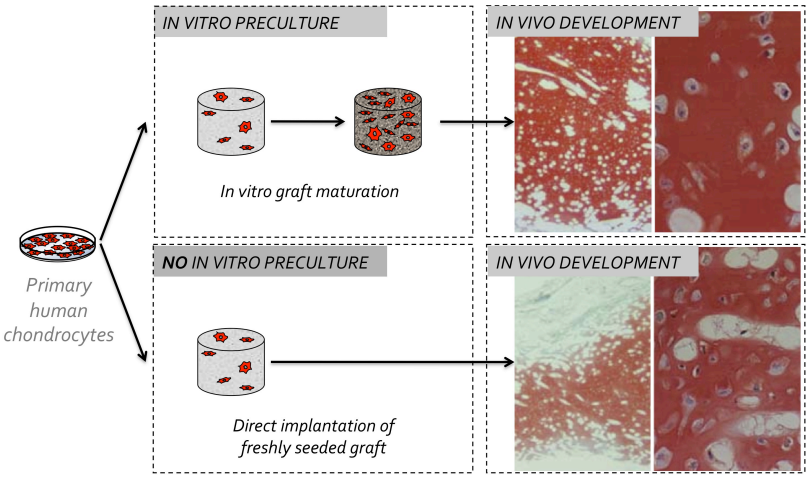

Figure 11 Cartilage tissue engineering: exemplification of modularity of tissue development and requirement of pre-cultivation of the graft to achieve a certain degree of maturation (results taken from Moretti et al 2005)

3.2.2 Cartilage tissue engineering

As a breakthrough in the field of cartilage regeneration, in 1994 Brittberg and colleagues introduced a new procedure, so called Autologous Chondrocyte Transplantation (ACT). The patient undergoes two joint surgeries: the first to harvest a cartilage biopsy from which autologous chondrocytes can be isolated and the second to re-implant the autologous chondrocyte graft to repair the defect. This cell-based method relies on (i) in vitro expansion of autologous chondrocytes prior to injection at the defect site as a cell suspension or—in an improved version—in association with a supportive matrix (matrix-assisted ACT, MACT) and on (ii) chondrocyte capacity to reconstitute the native matrix once back in vivo (Brittberg 1999; Pelltari, Winxmerten, and Martin 2009). The clinical outcome of these chondrocyte-based techniques is generally good, as they lead to decreasing of symptoms for the patient but in many

cases results in the formation of inferior fibrous repair tissue in terms of mechanical properties and durability. Different aspects of this clinical procedure have been implemented in the recent years. On one side, it has been questioned whether in vitro maturation of the graft is required (Moretti, et al. 2005 and figure 11) by formulating the question “how good is good enough?” in terms of product quality and clinical outcome. Indeed, chondrogenic pre-cultivation is key to (i) improve donor cell retention, (ii) possibly protect cells from inflammatory reaction at the repair site, (iii) enhance in vivo development, (iv) improve cellular response to mechanical loading and, (v) from the clinical point of view, guarantee easier surgical handling and possibly earlier postoperative loading (Pelttari, Wixmerten, and Martin 2009).

On the other side, product manufacturing pipeline could be improved, simplified and streamlined: a remarkable example of single closed system for graft production is the device ACTES (Autologous Clinical Tissue Engineering System) currently under development by Octane, which is an automated bioreactor where autologous cartilage biopsy can be digested and isolated chondrocytes can be expanded before being seeded and cultured on an osteochondral porous scaffold prior to implantation.

3.2.3 Bioreactors in tissue engineering

Conventional tissue engineering pipelines are costly, labor-intensive and time consuming, due to their manual nature. Successful clinical use of engineered tissue products, as well as their commercial exploitation, might be critically dependent on the introduction of bioreactors. Bioreactors, intended as a means to generate and maintain controlled physicochemical culture environment, indeed represent key elements in developing automated, standardized, traceable, cost-effective, safe and regulatory-compliant manufacture of cell-based products or engineered grafts for clinical applications (Martin, Smith, and Wendt 2010).

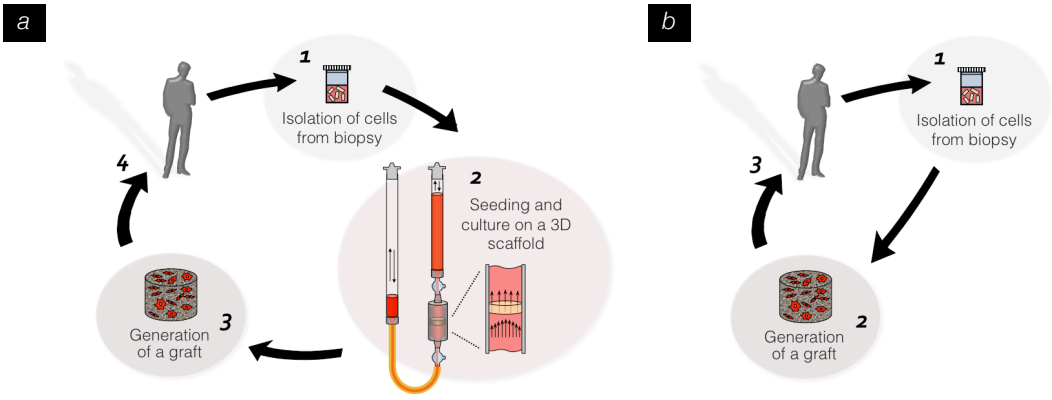

Figure 12 Examples of implementation of conventional tissue engineering paradigm by means of bioreactor systems. a) Bioreactors as tool to perform streamlined cell seeding and cell culture directly in 3D scaffold and within a single closed system. b) Bioreactor applied in intra-operative procedure and exploited to perform cell treatment directly prior to graft implantation.

Implementation of traditional tissue engineering paradigms passes through better control and standardization: this can be achieved, firstly, with automation of culture procedures by means of bioreactor systems.

Bioreactors, for instance perfusion bioreactors, are meant (i) to improve seeding and culture conditions of engineered constructs by enhancing mass transfer, (ii) to control and monitor critical culture parameters, (iii) to provide physical conditioning of developing tissues and (iv) to predict graft mechanical functionality.
Unlike conventional manual based procedures, bioreactors allow automation and streamlining of in vitro culture as depicted in Figure 12a, and up-scaling of graft and production for efficient clinical translation. In controlled closed bioreactor system, computational fluid dynamics can be applied to describe flow dependent processes as model-based simulations of velocity and shear stress profiles. This, in turn, could be fundamental to understand and optimise operating parameters and to predict culture outcome. Bioreactor based cultures might become robust 3D model systems, where external perturbations of culture parameters can be predicted and tuned to maintain system stability (Wendt, et al. 2009).
Moreover, the conventional tissue engineering paradigm we described could be further adjusted towards an intra-operative vision, if feasible. In this latter case, bioreactors could implement cell preparation step (i.e. biopsy treatment, cell isolation, combination with carrier) directly upon graft implantation (Figure 12b steps 1,2,3).

3.3 Developmental engineering concept

Nowadays, to the extent that the mechanisms of tissue development and repair are known, tissue engineering could undergo a major conceptual and methodological transformation: a change in the mindset of tissue engineers might move experiments from trial-and-error approaches to rigorous plans for regenerative medicine (Lenas, Moos, and Luyten 2009 part I and II).
In principle, the new paradigm in tissue engineering is no longer three-dimensional (3D) cell growth and differentiation but strict biomimetism, so that in vitro processes recapitulate key events of in vivo development and repair courses.
This strategy will allow fundamental understanding of what makes a tissue different than a 3D cellular graft and develop a methodology that can meet cost-effective, quality-validated, and clinically oriented process. In particular, substantial pieces of information on spatial-temporal organization of developing tissues and functions could be keys for graft manufacturing implementation.
As a matter of fact, the benefits of recapitulating complicated developmental stages in in vitro procedures might not be immediately captured: the process design point of view should be taken. The knowledge gained from developmental biology that can be incorporated into tissue engineering procedures can be summarized in (i) path-dependence of the steps, (ii) robustness of the system, (iii) modularity of the process, and (iv) semi-autonomy of intermediate tissue forms. For example, in the growth plate, tissue size and cell differentiation progression takes place in a well-orchestrated manner: each developmental step represents an independent module of the process which is robust and self established thanks to the tight

interconnection with previous and following steps.

The nature of the process directly allows for cell and functional organization. Cartilage and bone tissue engineering could be well adapted to this strategy and would potentially gain great benefits. Engineered graft production could incorporate the critical steps occurring in vivo, acquiring stability, reproducibility and controllability. The translation towards the so-called "developmental engineering" approach might pave the way to new generation graft manufacture (Lenas, Moos, and Luyten 2009 part I and II).

4. Experimental work

In the last years, different fields of investigation have risen from the initial concept of tissue engineering coined by Vacanti and Langer (Vacanti and Langer 1993). In our experimental work, we tried to merge together developmental engineering and bioreactor based approaches towards skeletal graft manufacturing implementation.

Firstly, we aimed to recapitulate embryological events occurring during endochondral bone formation to ultimately engineer bone grafts. We based our first hypothesis on the phenotypical instability of MSC when committed towards the chondrogenic lineage. As first demonstrated by Pelttari et al (Pelttari, et al. 2006), in vitro chondrogenesis of MSC leads to hyperthrophy, as direct consequence of initiation of endochondral route: this differentiation state is undesirable for cartilage tissue engineering purposes, where stability of formed cartilaginous tissue is mandatory for successful construct engraftment. On the contrary, the hyperthrophic state of MSC could be exploited for bone tissue engineering: thus, by analogy to embryonic limb development, we first hypothesized that adult human bone marrow derived MSC, a clinically compliant cell source, were able to recapitulate the steps of endochondral route (condensation, chondrogenesis, hyperthrophy, vasculogenesis coupled with tissue remodeling, and ultimately bone formation). Most importantly, this process could generate advanced grafts for bone regeneration by invoking a "developmental engineering" paradigm and provide a valid model to study mechanisms governing bone development (**Chapter I**).

We thus aimed at efficiently transferring the paradigm to a bioreactor-based approach, by exploiting modularity of endochondral pathway and semiautonomy of intermediate tissues. Each developmental milestone could be translated in specific controlled bioreactor in vitro phases, possibly up-scaling graft manufacturing and production. Therefore in the second part of the thesis, we focused on streamlining the process, focusing on the first two events of endochondral route (i.e. condensation and chondrogenesis) and by means of a single closed bioreactor system. We first aimed at optimizing the development of cartilaginous graft by cell seeding, proliferation, condensation and chondrogenic differentiation directly in 3D scaffolds and by applying temporally defined and controlled perfusion regimes. Secondly we aimed at assessing the feasibility of up-scaling graft size, in the clinical context of unicompartimental joint cartilage repair (**Chapter II**).

Finally, we wanted to achieve robustness of each module of the endochondral route and we started from the

first step: we set a model system to study and specifically control initial cell condensation, directly in 3D porous scaffold within perfusion bioreactor system. It has been previously demonstrated how important is cell distribution upon scaffold seeding for subsequent tissue maturation (Wendt, et al. 2006) and it has been studied the importance of cell density to prime chondrogenesis (Moretti, et al. 2005). We combined different complementary experimental approaches (biomaterial design, computational fluid dynamics and bioreactor based cell culture) and established a model system to study the correlation between changes in scaffold porosity, shear stress and cell distribution upon perfusion seeding. By smart scaffold design and proper perfusion regime we controlled cell distribution, with the ultimate goal to obtain the desirable cell density supporting proliferation or differentiation, in accordance to the developmental stage we aimed to recapitulate (**Chapter III**).

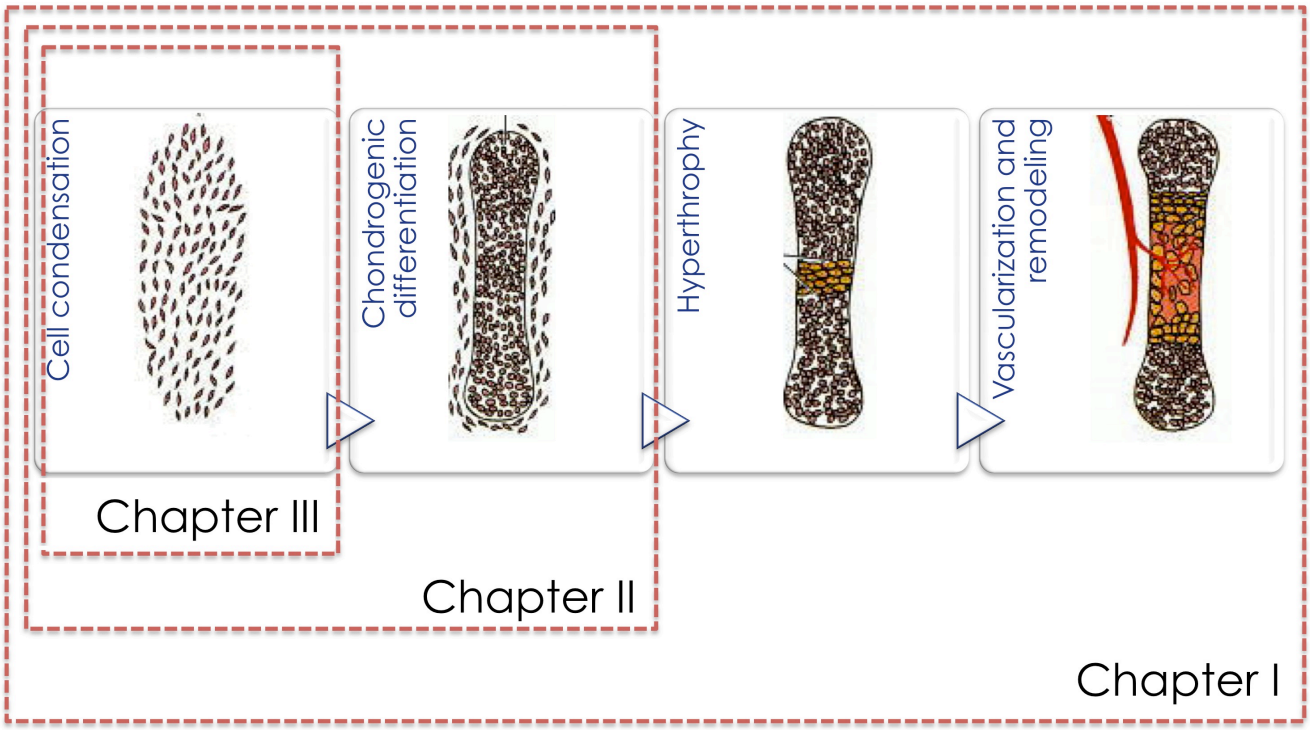

Recapitulation of the Aims of the experimental work:

Chapter I: *Recapitulation of embryological events that occur during endochondral bone formation to ultimately engineer bone constructs*

Chapter II: *Streamlining the first events of the endochondral route; Optimization of cartilaginous graft development by cell seeding, cell proliferation and chondrogenic differentiation directly in 3D scaffolds and within a single closed bioreactor system; Upscaling graft size for cartilage repair*

Chapter III: *Control of initial cell distribution in 3D matrices upon perfusion bioreactor seeding and therefore control of cell condensation phase in the context of endochondral graft manufacturing.*

References

Axelrad TW, Einhorn TA. "Bone morphogenetic proteins in orthopaedic surgery." Cytokine Growth Factor Rev. 20, no.5-6 (2009):481-8.

Bailon-Plaza A, and Van der Meulen MCH "A Mathematical Framework to Study the Effects of Growth Factor Infuences on Fracture Healing." J. theor. Biol. 212 (2001): 191-209.

Bianco P, De Scalzi Cancedda F, Riminucci M, and Cancedda R. "Bone Formation via Cartilage Models: The "Borderline" Chondrocyte." Matrix Biology 17 (1998): 185-192.

Braccini A, et al. "Three-dimensional perfusion culture of human bone marrow cells and generation of osteoinductive grafts." Stem Cells 23, no. 8 (2005): 1066-72.

Brittberg M. "Autologous chondrocyte transplantation." Clin Orthop Relat Res., no. 367 (1999): S147-55.

Colnot C, et al. "Altered fracture repair in the absence of MMP9." Development 30, no.17 (2003): 4123-33

Day TF, and Yang Y. "Wnt and Hedgehog Signaling Pathways in Bone Development." The Journal Of Bone And Joint Surgery 90, no. 1 (2008): 19-24.

Eames BF, de la Fuente L, and Helms JA. "Molecular Ontogeny of the Skeleton." Birth Defects Research (Part C) 69 (2003): 93-101.

Gerstenfeld LC, et al. "Fracture healing as a postnatal developmental process: molecular, spatial, and temporal aspects of its regulation." Journal of cellular biochemistry 88 (2003): 873-884.

Hall BK, and Miyake T. "All for one and one for all: condensations and the initiation of skeletal development." BioEssays 22 (2000): 138–147.

Horton WA, and Degnin CR. "FGFs in endochondral skeletal development." Trends in Endocrinology and Metabolism 20, no. 7 (2009).

Kronenberg HM. "Developmental regulation of the growth plate." Nature 423, no. 15 (2003).

Lenas P, Moos M, and Luyten FP. "Developmental Engineering: A New Paradigm for the Design and Manufacturing of Cell-Based Products. Part I: From Three-Dimensional Cell Growth to Biomimetics of In Vivo Development." Tissue engineering Part B 15, no. 4 (2009): 381-394.

Lenas P, Moos M, and Luyten FP. "Developmental Engineering: A New Paradigm for the Design and Manufacturing of Cell-Based Products. Part II. From Genes to Networks: Tissue Engineering from the Viewpoint of Systems Biology and Network Science." Tissue engineering: Part B 15, no. 4 (2009): 395-422.

Leucht P, et al. "Translating insights from development into regenerative medicine: The function of Wnts in bone biology." Seminars in Cell & Developmental Biology 19 (2008): 434–443

Maes C, et al. "Osteoblast precursors, but not mature osteoblasts, move into developing and fractured bones along invading blood vessels." Developmental Cell 19 (2010): 329-344.

Martin I, Smith T, and Wendt D. "Bioreactor-based roadmap for the translation of tissue engineering strategies into clinical products" Trends in Biotechnology 27, no. 9 (2009): 495-502.

Moretti M, et al. "Effects of in Vitro Preculture on in Vivo Development of Human Engineered Cartilage in an Ectopic Model." Tissue Engineering 11, no. 9/10 (2005): 1421-8.

Pelttari K, Wixmerten A, and Martin I. "Do we really need cartilage tissue engineering?" Swiss Med Wkly 139, no. 41-42 (2009): 602-609.

Pelttari K, Steck, E and Richter W. "The use of mesenchymal stem cells for chondrogenesis." Injury, Int. J. Care Injured, 39S1 (2008): S58–S65.

Pelttari K, et al. "Premature induction of hyperthrophy during in vitro chondrogenesis of human mesenchymal stem cells correlates with calcification and vascular invasion after ectopic transplantation in SCID mice." Arthritis and Rheumatism 54, no. 10 (2006): 3254-66.

Quintana L, zur Nieden NI, and Semino CE. "Morphogenetic and Regulatory Mechanisms During Developmental Chondrogenesis: New Paradigms for Cartilage Tissue Engineering." Tissue Engineering 15 (2009): 29-41.

Salgado AJ, Coutinho OP, Reis RL. "Bone Tissue Engineering: State of the Art and Future Trends." Macromol. Biosci. 4, (2004): 743–765

Scherberich A, et al. "Three dimensional perfusion culture of human adipose tissue-derived endothelial and osteoblastic progenitors generates osteogenic constructs with intrinsic vascularization capacity." Stem cells 25, no. 7 (2007): 1823-9.

Scotti C, et al. "Recapitulation of endochondral bone formation using human adult mesenchymal stem cells as a paradigm for developmental engineering." PNAS 107, no. 16 (2010): 7251-6.

Shapiro F. "Bone development and its relation to fracture repair. The role of mesenchymal osteoblasts and surface osteoblasts." Eu Cells and Materials 15 (2008): 53-76.

Sundelacruz S, and Kaplan DL. "Stem cell- and scaffold-based tissue engineering approaches to osteochondral regenerative medicine." Seminars in Cell & Developmental Biology 20 (2009): 646-655.

ten Berge D, Brugmann SA, Helms JA, and Nusse R. "Wnt and FGF signals interact to coordinate growth with cell fate specification during limb development." Development 135 (2008): 3247-3257.

Vacanti JP, and Langer R. "Tissue engineering" Science 260 (1993): 920-926.

Wendt D, et al. "Uniform tissues engineered by seeding and culturing cells in 3D scaffolds under perfusion at defined oxygen tensions." Biorheology 43, no. 3-4 (2006): 481-8.

Wendt D, et al. "Potential and bottlenecks of bioreactors in 3D cell culture and tissue manufacturing." Advanced Materials 21 (2009): 1-16.

Zelzer E, and Olsen BR. "The genetic basis for skeletal diseases." Nature 423 (2003): 343-348

Chapter I

Engineering Cartilaginous Template For Endochondral Ossification

"Recapitulation of endochondral bone formation using human adult mesenchymal stem cells as a paradigm for developmental engineering"

Enclosed is the pdf-file of the Paper published in Proc Natl Acad Sci U S A, 2010, Apr; 107(16): 7251-6

Recapitulation of endochondral bone formation using human adult mesenchymal stem cells as a paradigm for developmental engineering

Celeste Scotti[a,b,1], Beatrice Tonnarelli[a,1], Adam Papadimitropoulos[a], Arnaud Scherberich[a], Stefan Schaeren[a], Alexandra Schauerte[c], Javier Lopez-Rios[c], Rolf Zeller[c], Andrea Barbero[a,2], and Ivan Martin[a,2]

[a]Departments of Surgery and of Biomedicine, University Hospital Basel, Hebelstrasse 20, 4031 Basel, Switzerland; [b]Residency Program in Orthopaedics and Traumatology, Università degli Studi di Milano, Milan, Italy; and [c]Developmental Genetics, Department of Biomedicine, University of Basel, Mattenstrasse 28, 4058 Basel, Switzerland

Edited* by Robert Langer, Massachusetts Institute of Technology, Cambridge, MA, and approved February 18, 2010 (received for review January 12, 2010).

Mesenchymal stem/stromal cells (MSC) are typically used to generate bone tissue by a process resembling intramembranous ossification, i.e., by direct osteoblastic differentiation. However, most bones develop by endochondral ossification, i.e., via remodeling of hypertrophic cartilaginous templates. To date, endochondral bone formation has not been reproduced using human, clinically compliant cell sources. Here, we aimed at engineering tissues from bone marrow-derived, adult human MSC with an intrinsic capacity to undergo endochondral ossification. By analogy to embryonic limb development, we hypothesized that successful execution of the endochondral program depends on the initial formation of hypertrophic cartilaginous templates. Human MSC, subcutaneously implanted into nude mice at various stages of chondrogenic differentiation, formed bone trabeculae only when they had developed in vitro hypertrophic tissue structures. Advanced maturation in vitro resulted in accelerated formation of larger bony tissues. The underlying morphogenetic process was structurally and molecularly similar to the temporal and spatial progression of limb bone development in embryos. In particular, Indian hedgehog signaling was activated at early stages and required for the in vitro formation of hypertrophic cartilage. Subsequent development of a bony collar in vivo was followed by vascularization, osteoclastic resorption of the cartilage template, and appearance of hematopoietic foci. This study reveals the capacity of human MSC to generate bone tissue via an endochondral program and provides a valid model to study mechanisms governing bone development. Most importantly, this process could generate advanced grafts for bone regeneration by invoking a "developmental engineering" paradigm.

bone repair | endochondral ossification | hypertrophic chondrocytes | regenerative medicine | tissue engineering

Long bones and the axial skeleton in the developing embryo are formed by endochondral ossification, namely, by remodeling of cartilage templates (1). This process relies on the specialized morphoregulatory functions of hypertrophic chondrocytes (2). Hypertrophic chondrocytes derive from the condensation of mesenchymal precursors and produce a type X collagen-rich avascular cartilaginous matrix. At the periphery of this cartilage tissue, the so-called "borderline" hypertrophic chondrocytes (3) instruct surrounding mesenchymal cells to differentiate into osteoblasts, which results in the formation of a "bony collar." In parallel, chondrocytes in the central regions direct mineralization of the hypertrophic cartilage by initiating remodeling via the production of specific matrix metalloproteinases (MMP) and attract blood vessels by releasing vascular-endothelial growth factor (VEGF). The in-growing blood vessels deliver osteoblastic, osteoclastic, and hematopoietic precursors, which mediate resorption of the cartilaginous template and formation of vascularized bone containing the so-called stromal sinusoids, which provide the microenvironment for hematopoiesis (1).

Mesenchymal stem/stromal cells (MSC) from human adults have the ability to generate bone tissue in a variety of experimental models (4), and hold great potential in regenerative medicine. Thus far, MSC have been shown to generate bone exclusively through direct osteogenic differentiation (i.e., in a manner akin to intramembranous ossification), using a mineralized surface as "priming" substrate, with the exception of implantation in confined environments that prevent blood vessel invasion (e.g., diffusion chambers; refs. 5 and 6). This approach has already been used for a few clinical trials (7) but has not been effective for widespread clinical application (4). The possibility to engineer MSC-based grafts recapitulating the morphogenetic processes of endochondral ossification of embryonic skeletogenesis would represent an important step forward for bone repair, in line with the recently defined "developmental engineering" concepts (8). In particular, the proposed route to bone formation through cartilage remodeling and vascularization, which is also activated during fracture repair, would potentially overcome issues critical to the physiological functioning of engineered bone grafts, such as osteogenic performance, resistance to hypoxic conditions, and efficiency of engraftment. So far, evidences of ectopic bone tissue morphogenesis via formation of hypertrophic cartilage templates have been reported for murine embryonic stem cells (ESC) (9) and chick embryonic mesenchymal cells (10), but the paradigm has thus far not been reproduced using human ESC or clinically potentially more relevant sources such as adult human MSC (9). The present study aimed at establishing and characterizing an endochondral bone tissue engineering approach, which uses bone marrow-derived, human adult MSC. By analogy to the development of long bones, we hypothesized that the stage of hypertrophy reached in vitro by MSC would critically impact on the process of endochondral ossification following implantation. Our results demonstrate that engineered human hypertrophic cartilaginous tissue has the potential to undergo developmental changes similar to the ones during limb formation. Therefore, this study paves the way toward a "developmental engineering" approach for the regeneration of bone.

Author contributions: C.S., B.T., A.P., A. Scherberich, A. Schauerte, J.L.-R., R.Z., A.B., and I.M. designed research; C.S., B.T., A.P., A. Schauerte, J.L.-R., and A.B. performed research; S.S. contributed new reagents/analytic tools; C.S., B.T., A.P., A. Scherberich, A. Schauerte, J.L.-R., R.Z., A.B., and I.M. analyzed data; and C.S., B.T., A. Scherberich, J.L.-R., R.Z., A.B., and I.M. wrote the paper.

The authors declare no conflict of interest.

*This Direct Submission article had a prearranged editor.

[1]C.S. and B.T. contributed equally to this work.

[2]To whom correspondence may be addressed at: Institut für chirurgische Forschung und Spitalmanagement, University Hospital Basel, Hebelstrasse 20, Zentrum für Lehre und Forschung, Room 405, 4031 Basel, Switzerland. E-mail: imartin@uhbs.ch or abarbero@uhbs.ch.

This article contains supporting information online at www.pnas.org/cgi/content/full/1000302107/DCSupplemental.

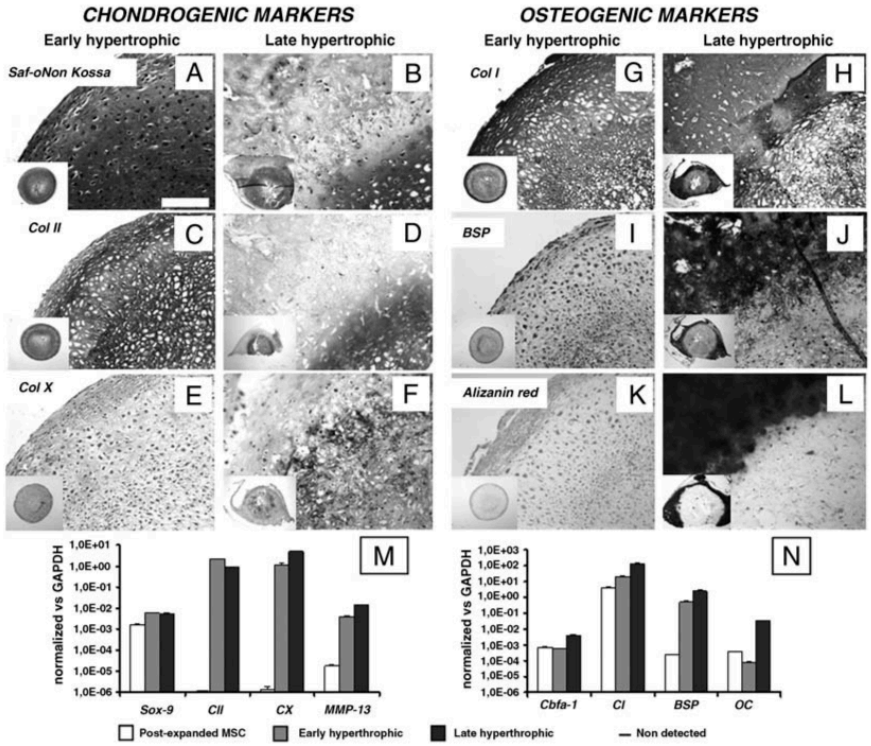

Fig. 1. In vitro maturation of hypertrophic cartilage tissues engineered from human adult MSC. In vitro culture conditions determined the composition and structure of the tissues generated. (*A*, *C*, *E*, and *G*) Early hypertrophic samples displayed a cartilaginous ECM rich in GAG and Col II with deposition of Col X and Col I in defined regions. (*I* and *K*) In the periphery of early hypertrophic samples, low BSP levels were detected, but no calcium was deposited. (*B*, *D*, *F*, *H*, *J*, and *L*) Late hypertrophic samples underwent further maturation in vitro and developed two distinct regions: an inner hypertrophic core (*B*, *D*, and *F*) rich in GAG, Col II, and Col X, and an outer mineralized rim (*B*, *H*, *J*, and *L*) with a high mineral content, Col I, and BSP. All pictures were taken at the same magnification. (Scale bar: 200 μm.) The insets display low magnification overviews of the entire tissues. (*M* and *N*) Quantitative real-time RT-PCR demonstrated an up-regulation of hypertrophic (Col X and MMP-13) and osteogenic (cbfa-1, OC, BSP) markers when comparing late with early hypertrophic tissues. Postexpanded MSC remained in an undifferentiated state but expressed both SOX-9 and Cbfa-1 in combination with high type I collagen and low type II collagen levels.

Results

In Vitro Maturation of Engineered Hypertrophic Cartilage Tissues. Since endochondral bone formation is initiated by condensation and chondrogenic differentiation of mesenchymal cells, we cultured human adult MSC in a transwell, scaffold-free system to maximize cell–cell interactions (11), using a serum-free medium supplemented with TGFβ1 as a potent inducer of chondrogenesis (12). After one week, the resulting tissues had deposited a loose extracellular matrix, which was faintly positive for glycosaminoglycans (GAG). These specimens will be hereafter referred to as "prechondrogenic" tissues. After 2 weeks, the resulting tissues displayed clear cartilaginous features, including positive Safranin-O staining for GAG (Fig. 1*A*) and large cells in lacunae embedded in abundant matrix (positive for type II collagen; Fig. 1*C*). As only low and localized levels of type X collagen, which marks hypertrophic chondrocytes, were detected (Fig. 1*E*), these specimens will be hereafter referred to as "early hypertrophic" tissues. At this stage, type I collagen was detected throughout the tissue (Fig. 1*G*), with staining intensity increased in the outer rim. In this outer rim, low levels of bone sialoprotein (BSP) were also detected (Fig. 1*I*), but no sign of matrix mineralization was apparent (Fig. 1*K*). In order to induce a more mature hypertrophic phenotype in human MSC, cells were cultured for 3 weeks in chondrogenic medium as described above and then for a further 2 weeks in medium lacking TGFβ1, but supplemented with β-glycerophosphate and l-thyroxin (13, 14). This culture protocol maintained the chondrogenic features, namely, GAG and type II collagen expression (Fig. 1 *B* and *D*), but also promoted abundant and widespread accumulation of type X collagen (Fig. 1*F*). The outer rim of the specimens was uniformly positive for type I collagen (Fig. 1*H*) and developed a distinct mineralized collar (Fig. 1*L*), strongly positive for BSP (Fig. 1*J*). This histological pattern is characteristic of what was previously defined as "chondro-osseous rudiment" (15), and therefore specimens at this stage will be hereafter referred to as "late hypertrophic" tissues. The progression of chondrogenesis through hypertrophy and mineralization between 2 and 5 weeks of in vitro culture was paralleled by increased expression of type X collagen (*CX*; 4.2-fold), *MMP13* (3.7-fold), core-binding factor alpha subunit 1 (*Cbfa1*; 7.2-fold), osteocalcin (*OC*; 430-fold), and BSP (*BSP*; 5.7-fold) transcripts (Fig. 1 *M* and *N*). Following hypertrophic differentiation, phenotypic analysis by cell flow cytometry demonstrated an overall decrease in the expression of markers typical for undifferentiated MSC (CD73, CD90, CD105, CD146) and an increase of alkaline phosphatase (ALP; Fig. S1). VEGF transcript, released protein, and matrix-bound protein were detected at similar levels throughout the culture stages (Fig. S2).

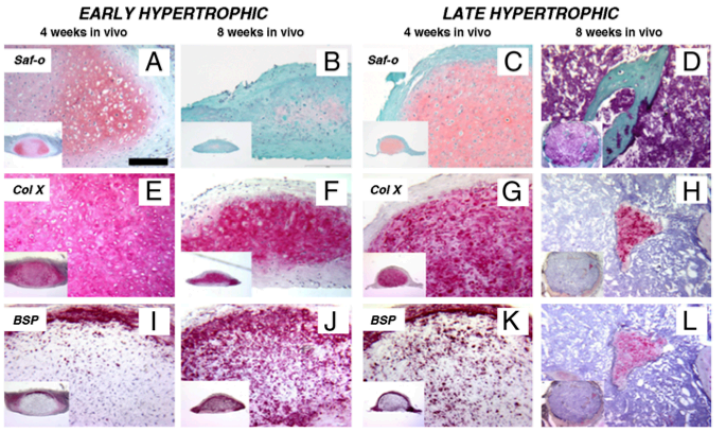

Fig. 2. Development of the hypertrophic cartilage tissues following in vivo implantation. The differentiation of cartilaginous constructs in vivo progressed according to their stage of in vitro maturation. (*A*, *E*, and *I*) Four weeks after implantation, early hypertrophic samples had differentiated further toward hypertrophy, displaying larger lacunae, Col X accumulation, and initiated BSP deposition in the outer rim. (*B*, *F*, and *J*) Eight weeks after implantation, early hypertrophic samples had differentiated even further. This was evidenced by a decrease in GAG accumulation, while Col X was maintained and BSP had also been deposited within the cartilaginous core. (*C*, *G*, and *K*) After 4 weeks, late hypertrophic specimens had undergone more intense remodeling, such that GAG and Col X levels were reduced, while BSP had already been deposited within the cartilaginous core. (*D*, *H*, and *L*) After 8 weeks, the cartilaginous template was almost completely resorbed: Bone structures substituted the GAG positive areas in the central region, while Col X and BSP positive areas were restricted to scattered islands. All the pictures were taken at the same magnification. (Scale bar: 200 μm.)

Progression of Bone Development Following in Vivo Implantation of Hypertrophic Cartilage Constructs. Prechondrogenic, early hypertrophic, and late hypertrophic constructs were implanted subcutaneously into nude mice and harvested after 4 and 8 weeks. Prechondrogenic constructs could not be recovered following implantation, as they were likely resorbed by the host environment. Following 4 weeks in vivo, early hypertrophic samples developed into structures containing cells embedded in large lacunae within an extracellular matrix rich in GAG (Fig. 2*A*) and type X collagen (Fig. 2*E*), while BSP deposition was confined in the outer rim (Fig. 2*I*). Eight weeks after implantation, the extracellular matrix was extensively remodeled and displayed reduced GAG levels (Fig. 2*B*) and diffused deposition of BSP (including the central regions, Fig. 2*J*). In the central region BSP overlapped with type X collagen (compare Fig. 2*J* to Fig. 2*F*). Four weeks after implantation, late hypertrophic samples displayed two distinct regions: an outer osteoid tissue, which resembled a bony collar, and an inner cartilaginous region, which was faintly positive for GAG (Fig. 2*C*). Type X collagen was present predominantly in the pericellular space (Fig. 2*G*), partially overlapping the accumulation of BSP (Fig. 2*K*). After 8 weeks in vivo, the cartilaginous template was almost completely resorbed, and bone ossicles appeared also in the central region (Fig. 2 *D*, *H*, and *L*). Taken together, these results indicate that (*i*) a hypertrophic cartilaginous template is required to prime the endochondral process, and (*ii*) the maturation of early hypertrophic samples toward the endochondral route progresses upon in vivo implantation, albeit it being delayed in comparison to implantation of late hypertrophic tissues.

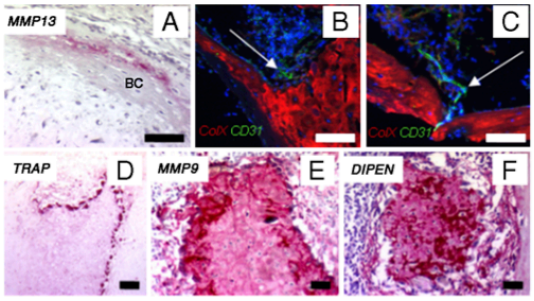

Fig. 3. In vivo remodeling and vascularization of late hypertrophic cartilage implants. (*A*) The observed remodeling resembles the temporal and spatial changes indicative of ongoing endochondral ossification. Hypertrophic chondrocytes located in the bony collar (BC) synthesized MMP13, which is known to prepare the ECM for vascular invasion during endochondral ossification. (*B* and *C*) Newly formed vessels, identified by CD31+ endothelial cells, penetrated the outer matrix and reached the inner core in close proximity to the cartilaginous areas undergoing remodeling (arrows). (*D* and *E*) The cartilaginous regions were colonized by TRAP-positive cells synthesizing MMP9. (*F*) These regions were also positive for the DIPEN, which is produced by MMP-mediated cleavage of aggrecan. (Scale bar: 100 μm.)

In Vivo Remodeling and Vascularization of Late Hypertrophic Cartilage. To assess if the progression of tissue morphogenesis in vivo closely resembled normal endochondral ossification, late hypertrophic specimens were analyzed in more detail. Four weeks after implantation, the outer regions corresponding to the bony collar were positive for MMP-13 (Fig. 3*A*), which is typically expressed by late hypertrophic chondrocytes or osteoblasts and acts upstream of initiating angiogenesis (16). Indeed, capillary vessels positive for CD31 (PECAM-1) began to penetrate the outer matrix (Fig. 3 *B* and *C*), consistent with the requirement to transport host osteoclasts, nutrients and proapoptotic signals to the internal hypertrophic cartilaginous template (1, 17). After 8 weeks in vivo, cartilaginous regions undergoing remodeling were surrounded by multinucleated cells of the osteoclastic lineage, as revealed by their positive staining for two markers typically expressed at this stage of resorption (18), namely, tartrate-resistant acid phosphatase (TRAP; Fig. 3*D*) and MMP-9 (Fig. 3*E*). The ongoing, active matrix digestion process was confirmed by abundant expression of the so-called cryptic epitope of aggrecan (DIPEN; Fig. 3*F*), which is exposed specifically upon MMP-mediated cleavage of aggrecan.

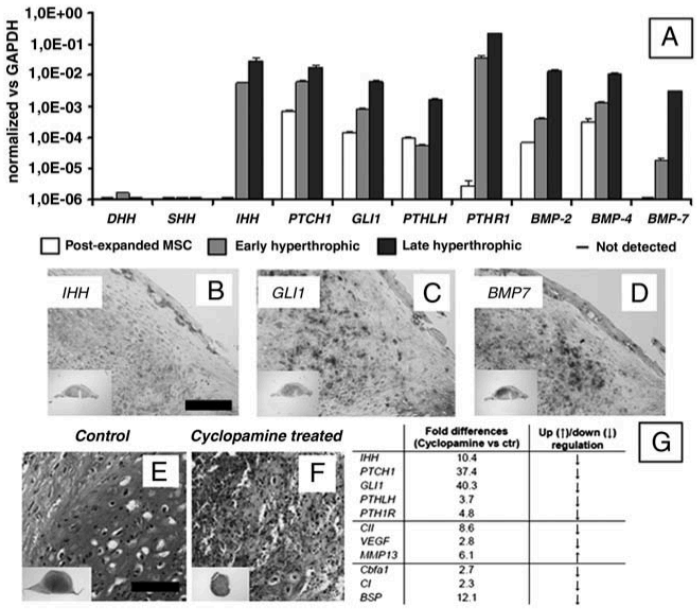

Fig. 4. Activation of signaling pathways involved in endochondral bone formation in embryos. Signaling pathways typically involved in endochondral ossification were activated in the engineered samples. (*A*) Real-time RT-PCR analysis indicated that MSC cultured under hypertrophic conditions up-regulated the expression of genes in the IHH signaling pathway (involving IHH, GLI1, and PTCH1), BMPs and parathyroid hormone-related protein signaling (PTHLH, PTHR1). Note that all fold changes in transcript levels are shown in logarithmic scale. (*B–D*) Four weeks after implantation, the expression of representative genes was assessed by ISH (IHH, GLI1, and BMP7). (*E–G*) Functional inhibition of the IHH pathway by cyclopamine treatment significantly reduced the expression of genes involved in IHH signaling (IHH, GLI1, PTCH1), PTH signaling (PTHLH, PTHR1), as well as chondrogenic/hypertrophic genes (Col II, VEGF), and osteogenic genes (Cbfa-1, Col I, BSP). Cyclopamine also blocked the differentiation and maturation of the cartilaginous templates in vitro, as assessed by Safranin-O stain. [Scale bar: 200 μm (*B–D*).] [Scale bar: 400 μm (*E* and *F*)].

Activation of Pathways Involved in Normal Endochondral Ossification. We next performed a real-time RT-PCR and in situ hybridization (ISH) analysis of the expression of key components of pathways that are known to be required for normal endochondral ossification (19–21). In particular, the expression of Indian hedgehog (IHH) as upstream signal, its receptor Patched1 (PTCH1), and GLI1 as mediator of IHH signal transduction was assessed. As expected, all these genes were either not expressed or expressed at very low levels in postexpanded MSC, while their expression levels were markedly increased in the early hypertrophic and even more in the late hypertrophic constructs (IHH 5.2-fold, PTCH1 3.0-fold, GLI1 7.8-fold—when comparing late to early hypertrophic tissues; Fig. 4*A*). In contrast, the expression of the other two hedgehog ligands present in vertebrate species including humans (sonic hedgehog SHH and desert hedgehog DHH) was not activated (Fig. 4*A*). Similar to IHH, bone morphogenetic proteins (BMPs) (BMP-2 36.5-fold, BMP-4 7.8-fold, BMP-7 169.4-fold), Parathyroid hormone-related protein (PTHLH 30.8-fold), and its receptor (PTHR1 6.2-fold) were significantly up-regulated in late as compared to early hyperthrophic tissues (Fig. 4*A*). This shows that the progression toward endochondral ossification, both in vitro and in vivo, is paralleled by the activation and/or up-regulation of the key signaling pathways involved in endochondral bone formation during embryonic limb skeletal morphogenesis (Fig. 4 *A–D* and Fig. S3). The human specificity of the ISH probes further allows one to conclude that implanted cartilaginous templates included not only cells that provided signals initiating endochondral ossification (i.e., IHH), but also cells which responded to such signals (i.e., by expressing GLI1), and thus activated the required morphogenetic pathways (i.e., by expression of BMP-7). The functional importance of IHH signal transduction was further evidenced by the fact that its selective inhibition by cyclopamine administration (22) to in vitro cultured cartilaginous templates derived from human MSC completely blocked their morphogenesis and maturation (Fig. 4 *E–G*).

Characterization and Quantification of the Engineered Endochondral Bone. Quantitative microtomography (μCT) of explants confirmed that deposition of mineralized matrix in early hypertrophic samples was negligible at 4 weeks after implantation and remained confined to the outer rim at 8 weeks (Fig. 5 *A* and *B*). In contrast, late hypertrophic constructs contained abundant peripheral mineral deposits already at 4 weeks and displayed an interconnected network of trabeculae throughout the core at 8 weeks after implantation (Fig. 5 *C* and *D*). Not only the quantity (Fig. 5*E*) but also the stage of maturation of the mineralized matrix was more advanced in late hypertrophic tissues, as revealed by the significantly higher mineral density (Fig. 5*F*) at both time points and by the lamellar morphology of the osteoid (Fig. 5 *G* and *H*). The complete loss of type X collagen in the lamellar structures of late hypertrophic tissues after 8 weeks in vivo contrasted with the remaining expression and partial overlap with osteocalcin in the early hypertrophic constructs (Fig. 5 *I* and *J*). This result indicates that shortened maturation in vitro may delay progression of endochondral ossification in vivo. To further investigate whether prolonged maturation in vivo would be able to compensate for shorter periods of in vitro culture, early hypertrophic constructs were analyzed 11 weeks after implantation, which results in a total period of in vitro and in vivo development equal to late hypertrophic samples analyzed 8 weeks after implantation. Interestingly, early hypertrophic samples analyzed after

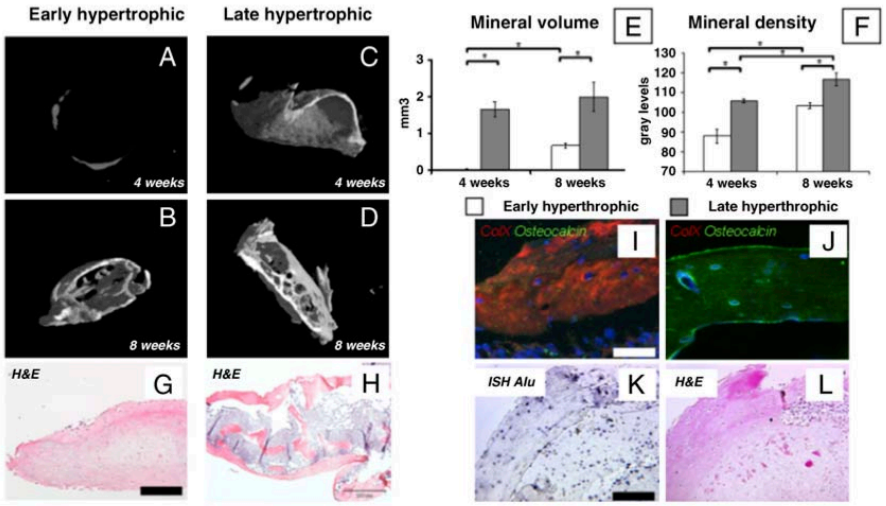

Fig. 5. Morphometric analysis of the engineered bone tissue. (*A–D*) Three-dimensional μCT reconstructions and (*E* and *F*) quantitative histomorphometric data ($n = 4$) of mineral volume and density indicate higher bone quantity and more advanced maturation of late hypertrophic samples (* indicates significant differences; $p < 0.01$). (*G* and *H*) Trabecular-like structures were found both in the outer bony collar and in the inner core of late, but not early, hypertrophic samples. (Scale bar: 200 μm.) (*I* and *J*) Fluorescence characterization for Col X (red) and osteocalcin (green) demonstrated the presence of mature lamellar bone only in late hypertrophic samples. (Scale bar: 50 μm.) (*K* and *L*) ISH to detect human *Alu* repeat sequences and hematoxylin/eosin staining of serial sections indicate that cells derived from the human adult MSC participated in the endochondral ossification process. (Scale bar: 100 μm.)

11 weeks displayed features of mature bone formation, although they remained significantly smaller than late hypertrophic constructs after 8 weeks of implantation (Fig. S4). It is currently debated whether the bone formed by endochondral ossification is exclusively generated by osteoblastic progenitors delivered by the vasculature or also by cells within the hypertrophic cartilaginous template (15). We thus assessed our explants by ISH for the presence of human *Alu* repeat sequences. The presence of positive cells within the trabeculae of the bone and the surrounding soft tissue demonstrates an active contribution of the human MSC in the newly formed bone tissue and thus an effective intrinsic osteogenic property of the engineered grafts (Fig. 5 *K* and *L*). Due to the nonclonality of the original human MSC population, our results are, however, not conclusive with respect to the controversial issue of whether bone cells derive by direct phenotypic conversion of hypertrophic chondrocytes or by direct osteoblastic differentiation of different MSC subsets (15). Endochondral skeletogenesis is known to generate a marrow microenvironment, which is prerequisite for hematopoiesis (23). Morphological analysis provided evidence for hematopoietic foci in some areas neighboring the bone matrix generated by the human adult MSC (Fig. S5*A*), which further validates the endochondral ossification process. Support for possibly ongoing hematopoiesis in these foci was provided by the presence of CD146+ stromal cells (24), which were detected in the tissue constructs (Fig. S5*B*).

Discussion

In this study, we report a hitherto not described capacity of adult expanded human MSC to generate de novo bone tissue in vivo through endochondral ossification. The observed endochondral morphogenesis bears striking features of normal endochondral ossification as is typical for limb skeletal development, namely, (*i*) cellular condensation and hypertrophic chondrogenesis, (*ii*) functional dependence on IHH signaling, (*iii*) formation of a bony collar by perichondral ossification, (*iv*) MMP-mediated matrix remodeling, vascularization, and osteoclastic activity, (*v*) bone matrix deposition over the resorbed cartilaginous template, and (*vi*) formation of complete bone tissue, which likely includes functional hematopoietic foci.

Our study shows that activation of the endochondral ossification program requires a mature hypertrophic cartilaginous template obtained in vitro (late hypertrophic constructs) or in vivo (early hypertrophic constructs), in which cells expressing high levels of type X collagen are surrounded by osteoblastic cells expressing high levels of BSP. These observations are consistent with the fact that the development of long bones is triggered by the formation of a vis-à-vis pattern between hypertrophic chondrocytes at the lateral aspects of the rudiment and differentiating osteoblasts in the surrounding mesenchymal tissues (25). Interestingly, the progression of bone formation in vivo was regulated by the developmental stage and size of the hypertrophic cartilaginous constructs generated in vitro for implantation. The need for a fine coordination between the stage of hypertrophy reached in vitro and the time required to achieve endochondral ossification in vivo is further confirmed by the reported absence of "frank" trabecular bone tissue in a previous study where chondrogenically differentiated human MSC were implanted ectopically (26).

The ectopic, "inert" subcutaneous implantation model used for this study allowed us to demonstrate that the hypertrophic cartilaginous constructs contained all necessary "biological instructions" to initiate a developmental process with similarities to what is observed during limb development (i.e., activation and up-regulation of IHH, BMP, and PTHLH signaling, and self-organization of the tissue in a spatially and temporally coordinated manner). The experimental concept described here is in line with the ideas of "developmental engineering," in that an engineered construct is able to progress through development and differentiation into a structured tissue in a manner comparable to normal progression of embryonic development (8). In particular, no instructive external signals seem required after implantation, and MSC were able to form bone tissue without a ceramic/mineral substrate, which is typically necessary to "prime" differentiation into functional osteoblasts (6, 27). This may open the possibility either to use the tissue itself as a scaffold (this study) or—in case a predefined size and shape is required—

to introduce different types of materials (e.g., synthetic polymers) that can be easier tailored with respect to their physical and/or mechanical properties and could be better biodegradable than ceramics (28).

By mimicking normal developmental processes during bone formation and repair, the endochondral route we describe here could provide significant biological and practical advantages in comparison to engineering approaches relying on intramembranous ossification. For example, implantation of a hypertrophic cartilage template, in contrast to a construct delivering undifferentiated MSC or osteoblasts, may be better suited to overcome the initial lack of vascularization and associated hypoxia. In fact, hypertrophic chondrocytes can accelerate graft invasion by blood vessels (e.g., by release of VEGF and production of MMPs) and are physiologically functional even at reduced oxygen tension (29). Moreover, considering the different composition and metabolism of bone tissues formed by intramembranous and endochondral morphogenesis (30), and the concept that bone repair processes should avoid major differences with normal developmental programs (31), MSC-driven bone formation via endochondral ossification could lead to more successful engraftment. Our study warrants further investigations toward a clinical implementation of the developed paradigm, including (*i*) scaling-up of the constructs implanted and (*ii*) orthotopic implantation in an immunocompetent animal model as biomechanical and inflammatory/immune mechanisms likely participate in regulating the bone forming potential of the hypertrophic templates. Finally, it will be interesting to assess the contribution of host cells in the observed processes, possibly in immunocompetent models (32), and if devitalized hypertrophic cartilage constructs might be able to initiate endochondral ossification by recruiting host progenitors. Experiments in this direction would open the attractive possibility to manufacture biological off-the-shelf grafts relying on the properties of a cell-laid extracellular matrix.

In conclusion, we describe a model based on human adult MSC, which recapitulates certain aspects of normal endochondral bone formation during embryonic development. The model system described is of clinical relevance for bone engineering and/or regeneration. Furthermore, it can be used to study the cellular/molecular mechanisms that control endochondral bone formation by human adult MSC isolated from both normal individuals and patients affected by specific diseases.

Materials and Methods

All human samples were collected with informed consent of the involved individuals and all mouse experiments were performed in accordance with Swiss law. All studies were approved by the responsible veterinary and ethics authorities. MSC were expanded for two passages and cultured in transwell (5×10^5 cells/insert) for 1 week or 2 weeks in a chondrogenic medium (with TGFβ1; prechondrogenic, and early hypertrophic, respectively), or for 3 weeks in chondrogenic medium followed by 2 weeks in a hypertrophic medium (without TGFβ1 and with beta-glycerophosphate and thyroxine; late hypertrophic). During in vitro culture, selected transwells were supplemented with 3-keto-N-(aminoethyl-aminocaproyl-dihydrocinnamoyl)-cyclopamine and cultured for 5 weeks. The resulting tissues were analyzed histologically, immunohistochemically, biochemically (GAG and DNA), and by real-time RT-PCR. Prechondrogenic, early hypertrophic, and late hypertrophic tissues were implanted subcutaneously in nude mice and retrieved after 4 or 8 weeks. Tissue development in vivo was evaluated histologically, immunohistochemically, and by μCT. The survival and contribution to bone formation by MSC was evaluated with ISH for human *Alu* sequences. Nonradioactive RNA ISH on paraffin sections (in vitro and in vivo constructs) was also performed using human antisense riboprobes specific for IHH, GLI1, and BMP7. A more complete and detailed description of the methods is included in *SI Text*.

ACKNOWLEDGMENTS. We are grateful to Silvia Reginato, Dr. Roberto Gianni-Barrera, and Dr. Andrea Banfi for the expert assistance with fluorescence and VEGF quantification; to Prof. Lee Ann Laurent Applegate and Prof. Dominique Pioletti for kindly providing human positive controls for ISH; and to Prof. Bert Mueller for the help in obtaining and interpreting μCT data. The work was partially funded by the Swiss National Science Foundation (Grants 310030-120432 to A. Scherberich and 31003A-113866 to R.Z.), by the European Space Agency (Grant "ERISTO" to I.M.) and by a European Marie Curie Reintegration Grant (PERG05-GA-2009-246576 to J.L.-R.).

1. Kronenberg HM (2003) Developmental regulation of the growth plate. *Nature* 423:332–336.
2. Noonan KJ, Hunziker EB, Nessler J, Buckwalter JA (1998) Changes in cell, matrix compartment, and fibrillar collagen volumes between growth-plate zones. *J Orthop Res* 16:500–508.
3. Bianco P, Cancedda FD, Riminucci M, Cancedda R (1998) Bone formation via cartilage models: The "borderline" chondrocyte. *Matrix Biol* 17:185–192.
4. Meijer GJ, de Bruijn JD, Koole R, van Blitterswijk CA (2007) Cell-based bone tissue engineering. *PLoS Med* 4:e9 doi:10.1371/journal.pmed.0040009.
5. Ashton BA, et al. (1980) Formation of bone and cartilage by marrow stromal cells in diffusion chambers *in vivo*. *Clin Orthop Relat Res* 151:294–307.
6. Martin I, Muraglia A, Campanile G, Cancedda R, Quarto R (1997) Fibroblast growth factor-2 supports ex vivo expansion and maintenance of osteogenic precursors from human bone marrow. *Endocrinology* 138:4456–4462.
7. Quarto R, et al. (2001) Repair of large bone defects with the use of autologous bone marrow stromal cells. *N Engl J Med* 344:385–386.
8. Lenas P, Moos MJ, Luyten F (2009) Developmental Engineering: A new paradigm for the design and manufacturing of cell based products. Part I: From three-dimensional cell growth to biomimetics of *in vivo* development. *Tissue Eng Pt B-Rev* 15:381–394.
9. Jukes JM, et al. (2008) Endochondral bone tissue engineering using embryonic stem cells. *Proc Natl Acad Sci USA* 105:6840–6845.
10. Oliveira SM, et al. (2009) Engineering endochondral bone: *In vivo* studies. *Tissue Eng Pt A* 15:635–643.
11. Murdoch AD, et al. (2007) Chondrogenic differentiation of human bone marrow stem cells in transwell cultures: Generation of scaffold-free cartilage. *Stem Cells* 25:2786–2796.
12. Johnstone B, Hering TM, Caplan AI, Goldberg VM, Yoo JU (1998) *In vitro* chondrogenesis of bone marrow-derived mesenchymal progenitor cells. *Exp Cell Res* 238:265–272.
13. Mackay AM, et al. (1998) Chondrogenic differentiation of cultured human mesenchymal stem cells from marrow. *Tissue Eng* 4:415–428.
14. Mueller MB, Tuan RS (2008) Functional characterization of hypertrophy in chondrogenesis of human mesenchymal stem cells. *Arthritis Rheum* 8:1377–1388.
15. Muraglia A, et al. (2003) Formation of a chondro-osseous rudiment in micromass cultures of human bone-marrow stromal cells. *J Cell Sci* 116:2949–2955.
16. Stickens D, et al. (2004) Altered endochondral bone development in matrix metalloproteinase 13-deficient mice. *Development* 131:5883–5895.
17. Gerber H-P, et al. (1999) VEGF couples hypertrophic cartilage remodeling, ossification and angiogenesis during endochondral bone formation. *Nat Med* 5:617–618.
18. Ortega N, Behonick D, Stickens D, Werb Z (2003) How proteases regulate bone morphogenesis. *Ann NY Acad Sci* 995:109–116.
19. St-Jacques B, Hammerschmidt M, McMahon AP (1999) Indian hedgehog signaling regulates proliferation and differentiation of chondrocytes and is essential for bone formation. *Genes Dev* 13:2072–86.
20. Karaplis AC, et al. (1994) Lethal skeletal dysplasia from targeted disruption of the parathyroid hormone-related peptide gene. *Genes Dev* 8:277–89.
21. Yoon BS, et al. (2005) Bmpr1a and Bmpr1b have overlapping functions and are essential for chondrogenesis *in vivo*. *Proc Natl Acad Sci USA* 102:5062–5067.
22. Taipale J, et al. (2000) Effects of oncogenic mutations in Smoothened and Patched can be reversed by cyclopamine. *Nature* 406:1005–1009.
23. Chan CK, et al. (2009) Endochondral ossification is required for haematopoietic stem-cell niche formation. *Nature* 457:490–494.
24. Sacchetti B, et al. (2007) Self-renewing osteoprogenitors in bone marrow sinusoids can organize a hematopoietic microenvironment. *Cell* 131:324–336.
25. Riminucci M, et al. (1998) Vis-à-vis cells and the priming of bone formation. *J Bone Miner Res* 13:1852–1861.
26. Pelttari K, et al. (2006) Premature induction of hyperthrophy during *in vitro* chondrogenesis of human mesenchymal stem cells correlates with calcification and vascular invasion after ectopic transplantation in SCID mice. *Arthritis Rheum* 54:3254–3266.
27. Haynesworth SE, Goshima J, Goldberg VM, Caplan AI (1992) Characterization of cells with osteogenic potential from human marrow. *Bone* 13:81–88.
28. Rezwan K, Chen QZ, Blaker JJ, Boccaccini AR (2006) Biodegradable and bioactive porous polymer/inorganic composite scaffolds for bone tissue engineering. *Biomaterials* 27:3413–3431.
29. Pfander D, Gelse K (2007) Hypoxia and osteoarthritis: How chondrocytes survive hypoxic environments. *Curr Opin Rheumatol* 9:457–462.
30. Van den Bos T, Speijer D, Bank RA, Brömme D, Everts V (2008) Differences in matrix composition between calvaria and long bone in mice suggest differences in biomechanical properties and resorption: Special emphasis on collagen. *Bone* 43:459–468.
31. Leucht P, et al. (2008) Embryonic origin and Hox status determine progenitor cell fate during adult bone regeneration. *Development* 135:2845–2854.
32. Tasso R, Fais F, Reverberi D, Tortelli F, Cancedda R (2009) The recruitment of two consecutive and different waves of host stem/progenitor cells during the development of tissue-engineered bone in a murine model. *Biomaterials* 31:2121–2129.

Supporting Information

Scotti et al. 10.1073/pnas.1000302107

SI Text

Materials and Methods. ***MSC isolation, in vitro culture, and in vivo implantation.*** Human mesenchymal stem cells (MSC) were isolated from ten bone marrow aspirates and processed as previously described (1). The two donors with the best chondrogenic potential, screened by means of micromass culture system (2), were chosen for the following experiments. MSC were expanded for two passages (referred to as postexpanded MSC) and differentiated into chondrogenic lineages in transwell culture (3) for 1 or 2 weeks in a serum-free chondrogenic medium (4), or for 3 weeks in chondrogenic medium followed by 2 weeks in a serum-free hypertrophic medium, supplemented with 50 nM thyroxine (5), 7.0×10^{-3} M β-glycerophosphate, 10^{-8} M dexamethasone, and 2.5×10^{-4} M ascorbic acid (2). Samples were implanted in subcutaneous pouches of nude mice (4 samples/mouse) and retrieved after 4, 8, or 11 weeks. During in vitro culture, selected transwells were supplemented with 5 μM 3-keto-N-(aminoethyl-aminocaproyl-dihydrocinnamoyl)-cyclopamine (Calbiochem), a potent derivative of cyclopamine (6) and cultured for 5 weeks.

Real-time RT-PCR quantitation of transcript levels. Total RNA extraction, cDNA synthesis (4) and real-time reverse transcriptase-polymerase chain reaction (RT-PCR; 7300 AB Applied Biosystem) were performed to quantitate expression levels of the following genes of interest: type II or type X collagen, bone sialoprotein (BSP), osteocalcin (4), Cbfa-1/Runx2 (Primer R GCC TTC AAG GTG GTA GCC C; Primer F CGT TAC CCG CCA TGA CAG TA; Probe CCA CAG TCC CAT CTG GTA CCT CTC CG), Matrix Metalloproteinase13 (MMP13-Applied Biosystems, Ref. number: Hs00233992_m1), desert hedgehog homolog (DHH-Applied Biosystems, Ref. number: Hs00368306_m1), sonic hedgehog homolog (SHH-Applied Biosystems, Ref. number: Hs01123832_m1), Indian hedgehog homolog (IHH-Applied Biosystems, Ref. number: Hs01081800_m1), patched homolog-1 (PTCH1-Applied Biosystems, Ref. number: Hs00970980_m1), glioma associated oncogene homolog −1 (GLI1-Applied Biosystems, Ref. number: Hs00171790_m1), parathyroid hormone-like hormone (PTHLH-Applied Biosystems, Ref. number: Hs00174969_m1),parathyroid hormone 1 receptor (PTH1R-Applied Biosystems, Ref. number: Hs00174895_m1), bone morphogenetic protein 2 (BMP2- Primer R AAC ACT GTG CGC AGC TTC C; Primer F CTC CGG GTT GTT TTC CCA C; Probe CCA TGA AGA ATC TTT GGA AGA ACT ACC AGA AAC TG), bone morphogenetic protein 4 (BMP4-Applied Biosystems, Ref. number: Hs00181626_m1), bone morphogenetic protein 7 (BMP7-Applied Biosystems, Ref. number: Hs00233476_m1). Glyceraldehyde 3-phosphate dehydrogenase (GAPDH) was used as housekeeping, reference gene (Primer R ATG GGG AAG GTG AAG GTC G; Primer F TAA AAG CAG CCC TGG TGA CC; Probe CGC CCA ATA CGA CCA AAT CCG TTG AC).

Histological staining and immunohistochemistry. After in vitro and in vivo cultures, the constructs were fixed in 1.5% paraformaldehyde, if necessary decalcified with 7% EDTA solution (Sigma) and embedded in paraffin. Sections (5 μm thick) were stained for Haematoxylin and Eosin (H&E) (Baker), Von Kossa in combination with Safranin-O (Fluka), Alizarin red, or for tartrate-resistant acid phosphatase (TRAP) activity by means of the leukocyte acid phosphatase kit (Sigma). Immunohistochemical analyses were performed to characterize the extracellular matrix over the time using the following antibodies: type I (Col I; MPBiomedicals), type II (Col II; MPBiomedicals), type X (Col X; AbCam) collagens, BSP (Immundiagnostik), MMP9 (AbCam), MMP13 (AbCam), Aggrecan cryptical epitope-DIPEN (MD Biosciences). Upon rehydratation in ethanol series, sections were treated as previously described for antigen retrieval for Col I and Col II (7), or according to the manufacturer's instructions. The immunobinding was detected with biotinylated secondary antibodies and using the appropriate Vectastain ABC kits. The red signal was developed with the Fast Red kit (Dako Cytomation) and sections counterstained by Haematoxylin. Negative controls were performed during each analysis by omitting the primary antibodies. Chromogenic in situ hybridization (CISH, Zytovision kit) to detect human *Alu* repeat sequences was performed following manufacturer's instructions. Histological and immunohistochemical sections were analyzed using an Olympus BX-61 microscope.

In situ hybridization. Nonradioactive RNA in situ hybridization analysis on paraffin sections (in vitro and in vivo constructs and human fetal bone) was performed as described (8), except that the RNase digestion step during the posthybridization washes was omitted. The human antisense riboprobes were synthesized using plasmids obtained from ImaGenes (human IHH: NM_002181.2; nt 1149-2041; GLI1: NM_005269.2; nt 2829-3595 and BMP7 : NM_001719.2; nt 3263 to 4049) and confirmed not to cross-react with murine transcripts.

Immunofluorescence images. Following in vivo implantation samples were fixed in 1.5% paraformaldehyde (Sigma), decalcified with EDTA (Sigma) solution, embedded in optimal cutting temperature, and snap frozen in liquid nitrogen. Sections (5 μm thick) were incubated with the primary antibodies against Col X (Abcam), osteocalcin (Millipore), CD31 (PECAM-1; BD Pharmingen), and PE-CD146 (BD Pharmingen). As appropriate, secondary antibodies labeled with Alexa Fluo 647, Alexa Fluo 488, Alexa Fluo 546 (Invitrogen) were used and DAPI was used to stain nuclei. Fluorescence images were acquired using an Olympus BX-61 microscope.

Microtomography. Microtomography was performed at different time points with in vivo implants. After fixation in formalin and storage in PBS, microtomography (μCT) data were acquired using a SkyScan 1174 table top scanner (SkyScan NV, Kontich, Belgium) with unfiltered x-rays (applied voltage 32 kV; current 800 μA). Transmission images were acquired during a 360° scan rotation with an incremental rotation step size of 0.4°. Reconstruction was made using a modified Feldkamp algorithm at an isotropic voxel size of 6.26 μm. Threshold-based segmentation and 3D measurement analyses (bone mineral density and volume) were performed using the CT-Analyzer program (SkyScan NV) as previously described (9). 3D rendering of the structures was performed using the VGStudio MAX 1.2.1 software.

Statistical analysis. The results of real-time RT-PCR and quantitative microtomography are presented as mean ±SD ($n = 4$). Statistical analysis was performed using the paired Student t-test (normality test $p > 0.05$). P-values of 0.05 or less were considered as statistically significant.

Flow cytometry. Cytofluorimetric analysis was performed after expansion of MSC and their differentiation in transwells. Expanded cells were treated with trypsin for 5 min at 37 °C, while tissues formed in transwells were trypsinized for 10 min at 37 °C, followed by 1.5% of collagenase digestion for 30 min at 37 °C in orbital shaker. The harvested cells were centrifuged (1500 rpm for 4 min) and the cell pellets incubated in dark at 4 °C for 30 min with antibodies against CD105 (Serotec), alkaline phosphatase (ALP, R&D), CD90, CD73, or CD146 (all from Becton Dickinson), and analyzed using a FACSCalibur flow cytometer (Becton Dickinson). Positive expression was defined by levels of fluorescence greater than 95% of corresponding isotype-matched control antibodies.

VEGF quantification. During culture, cell supernatants were collected at each medium change and analyzed for their content of VEGF protein (Quantikine, Human VEGF, R&D system). VEGF protein levels were also determined in total protein lysates collected from constructs cultured for 2 and 5 weeks. RNA extraction, cDNA synthesis (4), and real-time RT-PCR analysis were performed on constructs cultured for 2 and 5 weeks. VEGF transcript levels (Applied Biosystems, Ref. number: Hs00900055_m1) were determined by real-time PCR and normalized to the expression of GADPH.

1. Braccini A, et al. (2005) Three-dimensional perfusion culture of human bone marrow cells and generation of osteoinductive grafts. *Stem Cells*, 23:1066–1072.
2. Muraglia A, et al. (2003) Formation of a chondro-osseous rudiment in micromass cultures of human bone-marrow stromal cells. *J Cell Sci*, 116:2949–2955.
3. Murdoch AD, et al. (2007) Chondrogenic differentiation of human bone marrow stem cells in transwell cultures: Generation of scaffold-free cartilage. *Stem Cells*, 25:2786–2796.

4. Barbero A, Ploegert S, Heberer M, Martin I (2003) Plasticity of clonal populations of dedifferentiated adult human articular chondrocytes. *Arthritis Rheum*, 48:1315–1325.
5. Mackay AM, et al. (1998) Chondrogenic differentiation of cultured human mesenchymal stem cells from marrow. *Tissue Eng*, 4:415–428.
6. Taipale J, et al. (2000) Effects of oncogenic mutations in Smoothened and Patched can be reversed by cyclopamine. *Nature*, 406:1005–1009.
7. Dickhut A, et al. (2009) Calcification or dedifferentiation: Requirement to lock mesenchymal stem cells in a desired differentiation stage. *J Cell Physiol*, 219:219–226.
8. Chotteau-Lelièvre A, Dollé P, Gofflot F (2006) Expression analysis of murine genes using in situ hybridization with radioactive and nonradioactively labeled RNA probes. *Methods Mol Biol*, 326:61–87.
9. Papadimitropoulos A, et al. (2007) Kinetics of *in vivo* bone deposition by bone marrow stromal cells within a resorbable porous calcium phosphate scaffold: An X-ray computed microtomography study. *Biotechnol Bioeng*, 98:271–281.

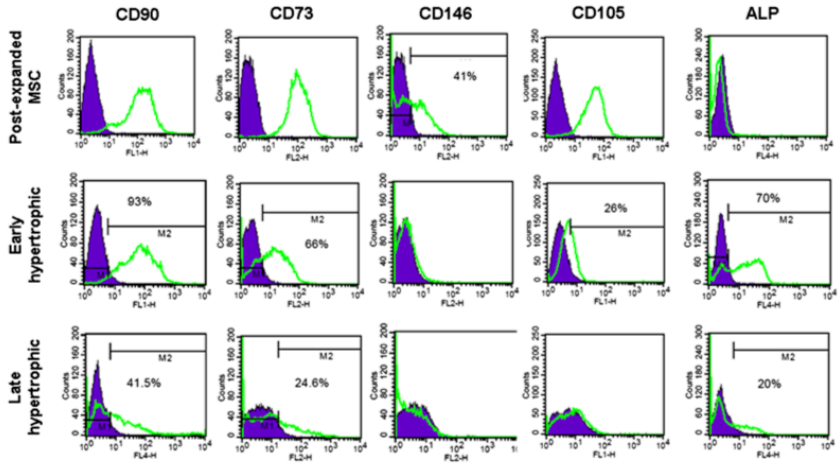

Fig. S1. Characterization of MSC by flow cytometry. After expansion, human MSC expressed typical MSC markers (CD90, CD73, CD146, CD105), but did not express ALP. During micromass culture in transwell plates, they gradually lost MSC markers and activated ALP expression.

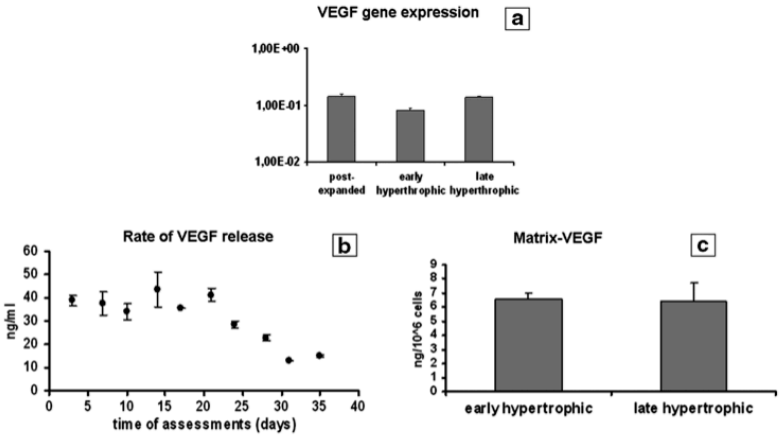

Fig. S2. Quantitation of VEGF transcripts and proteins. VEGF remained expressed under all experimental conditions. Quantitative real-time PCR reveals constant VEGF expression in postexpanded MSC and in early and late hypertrophic samples (*A*). VEGF protein was secreted into the culture medium and accumulated in the hypertrophic tissues (*B* and *C*).

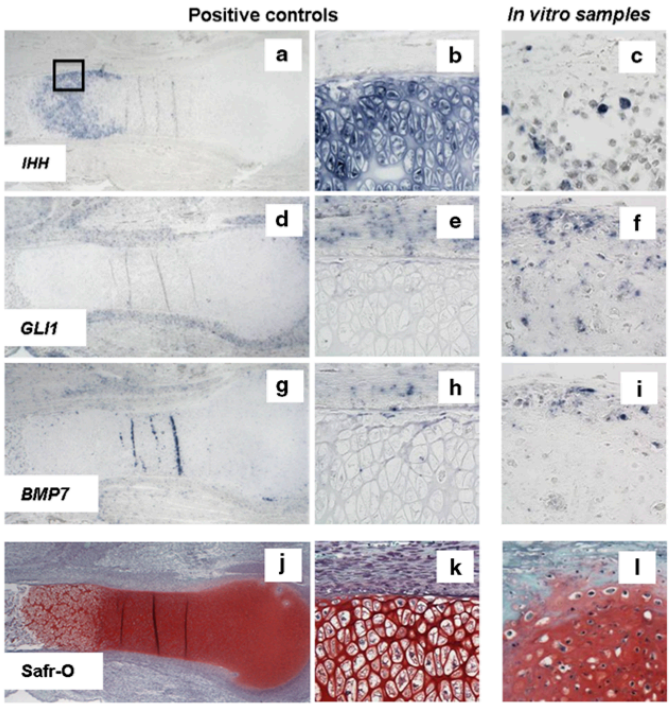

Fig. S3. Activation of signaling pathways in human foetal bone and in vitro cultured late hypertrophic samples. Paraffin sections of a human foetal bone specimens (about 2.5 months of gestation) were used as positive controls to detect the distribution of IHH (*A* and *B*), GLI1 (*D* and *E*), and BMP7 (*G* and *H*) transcripts by .in situ hybridization. Note the distribution of IHH transcripts in the hypertrophic chondrocytes (*A* and *B*) and GLI1 (*D* and *E*) and BMP7 (*G* and *H*) in the perichondrium. A reminiscent pattern was seen in the in vitro cultured late hypertrophic samples (5 weeks of culture; *C*, *F*, and *I*). Note that the activation of GLI1 in cells adjacent to IHH expressing cells is indicative of hedgehog signal transduction. Safranin-O staining on serial sections (*J*–*L*) was performed to reveal cell morphology and extracellular matrix structures in relation to the in situ hybridization results.

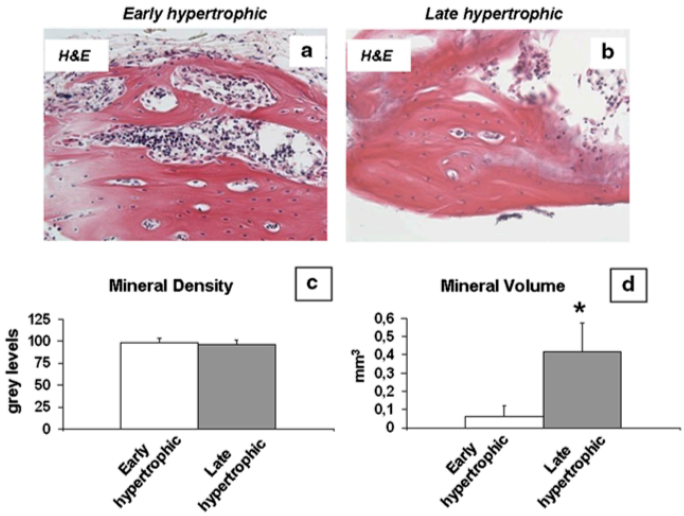

Fig. S4. Recovery of early hypertrophic samples upon prolonged in vivo culture. Development of early hypertropic constructs for the same total time as late hypertrophic samples (13 weeks, including 2 weeks in vitro and 11 in vivo) resulted in a similar extent of tissue maturation as revealed by histological analysis (*A* and *B*). Note the presence of both bone tissue and bone marrow-like regions. In addition, mineral densities were comparable as judged by μCT histomorphometry (*C*). However, the total mineral volume was significantly ($p < 0.01$) smaller, which is consistent with the smaller cartilage template generated during in vitro culture for only 2 weeks (*D*).

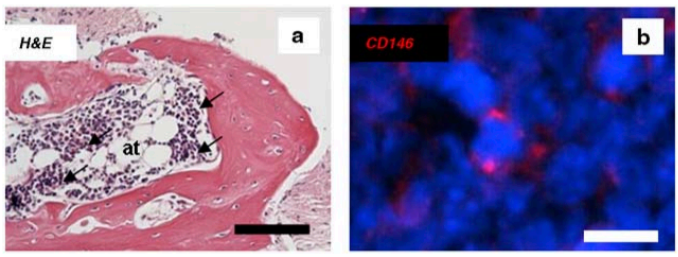

Fig. S5. Identification of bone marrow foci. Bone marrow structures were formed in the ossicles generated. Hematopoietic elements (*A*; arrow) (scale bar: 100 μm) and adipose tissue (*A*; at), together with CD146-positive cells (*B*) (scale bar: 5 μm), were found in proximity of the newly deposited bone matrix.

Chapter II

Novel Paradigm For Cartilage Graft Development Directly In 3D Scaffolds In Single Closed Bioreactor System

“Streamlined bioreactor based production of human cartilage tissue”

Beatrice Tonnarelli*, Rosaria Santoro*, Andrea Barbero, Ivan Martin and David Wendt.

University Hospital Basel, Switzerland.

* equally contributed authors

Enclosed is the Paper currently in preparation

Abstract

In the context of developmental tissue engineering for skeletal regeneration, we aim at recapitulating, optimizing and streamlining the first events of endochondral route (namely condensation and chondrogenesis), by combining specific signaling cues with 3D scaffold culture and bioreactor based approach. This protocol could be adapted both for endochondral and for cartilage tissue engineering. Therefore, as logical starting point, we hypothesized a clinical scenario for chondral graft generation, by using clinically relevant cell densities. Human articular chondrocyte (HAC) were isolated, efficiently expanded till chondrogenic permissive cell density was reached and further induced towards chondrogenic differentiation to deposit extracellular matrix rich in glicosamminoglicans (GAG) and collagen type II. All these steps where performed throughout 3D hyaluronan based meshes (Hyaff-11) and directly in the bioreactor system. Ultimately, we confirmed the feasibility of this approach with clinically sized constructs, by graft and bioreactor upscaling. Moreover, further developmental capacity of the generated graft was challenged in ectopic implants, demonstrating the importance of in vitro precultivation for graft stability. In comparison with conventional tissue engineering techniques relying on monolayer cell expansion (e.g., flask or petri dishes) and 3D construct culture in static conditions, bioreactor based cultures offer (i) comparable product quality, (ii) streamlined process so that less intensive manual labor and (iii) graft upscaling. Thus, the paradigm we introduced represents a remarkable step forward to translate engineered products and developmental engineering concept from bench to bedside.

Introduction

The novel trend of regenerative medicine is the recapitulation of the events occurring during tissue development along ex vivo manufacturing process. In line with this "developmental engineering paradigm", skeletal regeneration could undergo a major conceptual change: the generation of skeletal grafts might be implemented by mimicking the physiological steps of tissue formation, so that endochondral route (Lenas , Moos and Leutch 2009, I).

Therefore, the pipeline towards skeletal graft might pass through cell condensation by proliferation, chondrogenic differentiation, hyperthrophy, vascular ingrowth combined with matrix remodelling and, at last, bone formation.

The logical starting point for the implementation of this approach is the optimization and the streamlining of the first two events of this route (i.e. proliferation and chondrogenic differentiation).

As a matter of fact, the modularity of the process allows to translate this paradigm to cartilage graft manufacturing, an open clinical challenge where developmental engineering paradigm may be beneficial.

Lesions of articular joint surface might result in end-stage osteoarthritis and often require surgical interventions and total joint replacement by prosthesis. Modern tissue engineering approaches might offer an alternative paradigm for repair and regeneration of joint surface defects, in terms of clinical product and surgical procedures.

The conventional tissue engineering strategy to generate cartilage grafts typically relies on extensive in vitro monolayer proliferation (e.g., on flasks or Petri dishes) of the small number of cells that can be obtained from a typical sized biopsy, prior to cultivation within three dimensional (3D) scaffolds. Method associated with monolayer cell expansion and static culture of the graft are performed by specialised technicians, by using manual bench-top cell culture techniques. Although well established, these techniques (i) are labor-intensive, (ii) require specialised Good Manufacturing Practice (GMP) facilities, (iii) possess inherent safety risks, (iv) are challenged by intra-/inter-operator variability, and (v) have pragmatic limits on increasing unit production volumes (up-scaling), due to the manual nature of the procedures (Martin, Smith and Wendt 2009). A manufacturing process that bypasses the phase of monolayer cell expansion and static culture has the potential to generate engineered grafts with a more simplified and streamlined procedure, facilitating process automation within a single closed system.

In the context of bone regeneration, it has previously been shown that mesenchymal cells derived from a bone marrow aspirate (Braccini et al., 2005) or lipoaspirate (Scherberich et al., 2007) can be extensively expanded by loading the freshly isolated cells directly into a perfusion bioreactor and culturing the cells within the pores of a 3D scaffold, ultimately generating an engineered construct in a simple streamlined process which completely bypasses the phase of monolayer expansion.

In this work, we describe the adoption of the streamlined tissue engineering paradigm to produce cartilage grafts for small and large-scale cartilage defects and ultimately to recapitulate the first events of endochondral route. We specifically aim at simplifying conventional cell and tissue culture methods by using

bioreactor-based approach and at investigating cell proliferation and chondrogenic differentiation, directly within a three-dimensional biomaterial. We hypothesise to maintain the chondrogenic potential of human articular chondrocytes (HAC) - chosen as default cell source for cartilage tissue engineering- upon proliferation in 3D perfused scaffold (Hyaff-11 meshes), by switching the cellular phenotype with limited culture condition arrangements within a single closed bioreactor system.

Materials and methods

Cartilage Isolation:

Human articular cartilage samples were collected post mortem (within 24 hours after death), with informed consent and in accordance with the local Ethical Commission, from the knee joints of 8 individuals (mean age 63±5 years), with no history and no radiographic signs of joint disease. Human Articular Chondrocytes (HAC) were isolated using 0.15% type II collagenase for 22 hours and resuspended in Dulbecco's modified Eagle's medium (DMEM) containing 10% fetal bovine serum, 4.5 mg/ml D-Glucose, 0.1mM nonessential amino acids, 1mM sodium pyruvate, 100nM HEPES buffer, 100U/ml penicillin, 100ug/nl streptomycin, and 0.29mg/ml L-Glutamine (Complete Medium). Primary HAC were counted (average 2.92±0.12 E+06 cells/grams of biopsy) and directly used for the following experimental groups.

HAC Proliferation Phase:

Clinically applicable cell seeding densities were calculated based on data including an average size of a cartilage biopsy (up to 500 mg) (Brittberg, et al. 1994), the number of chondrocytes that can be obtained from a cartilage digest (2.5E+06 cells/gram cartilage) (Jakob, et al. 2003), and the dimensions of the clinically available engineered cartilage grafts based on hyaluronan acid: 1) Hyalograft-C® (2cm x 2cm x 0.2cm), usually used in the repair of small defects; and 2) larger scaffolds (5cm in diameter x 0.3cm), for large defect site (above $10cm^2$). Hyaff-11 meshes were either previously coated with fibronectin (concentration 50µg/ml), or remained uncoated to serve as controls.

In four independent experiments aiming at simulating the first clinical scenario (small graft generation), 1E+05 HAC were perfusion seeded onto 0.6cm in diameter x 0.2cm thick Hyaff-11® non-woven meshes (Fidia Advanced Biopolymers, FAB, Italy) at the clinically applicable cell density of 1.6E+06 cells/cm^3 scaffold volume, for 16 hours, at a perfusion rate of 1mm/s within a 10%CO_2/19%O_2 incubator. Following seeding, constructs remained in the bioreactor system (Wendt, et al. 2006) and were perfused at 100µm/s for an additional two weeks with "proliferating" culture medium (Complete Medium supplemented with 1ng/ml TGF $ß_1$ and 5ng/ml FGF-2).

In other four independent experiments designed to validate the large scaffold manufacturing process, 1E+06 HAC were perfusion seeded and expanded onto 5cm in diameter x 0.3cm thick Hyaff-11® non-woven

meshes at the clinically applicable cell density of 1.6E+05 cells/cm^3 scaffold volume in an up-scaled bioreactor system as previously described (Santoro, et al. 2010). Engineered constructs after proliferation phase were harvested for molecular biology, biochemistry, histological and immunohistochemical analyses.
Primary freshly isolated HAC were seeded at 5000 cells/cm^2 in conventional 2D culture flasks and expanded in monolayer as control for 3D expanded cells directly in bioreactors (Figure 1).

HAC Chondrogenic Differentiation Phase Upon Proliferation:

Following two weeks of perfusion culture under proliferating cultivation conditions, the oxygen level of the incubator was reduced from 19% to 5%O_2 to better support chondrocyte re-differentiation (Stroebel, et al. 2010), and constructs were perfused with "differentiating" culture medium (Complete Medium supplemented with 10ng/ml TGFß$_1$, 1UI/ml insulin, and 0.1mM ascorbic acid 2-phosphate) (Moretti, et al. 2005) for an additional two weeks. Monolayer expanded HAC underwent two passages along the 2 weeks of expansion culture and at the end of culture time were statically seeded onto 0.6cm in diameter x 0.2cm thick Hyaff-11® at the same cell density than the one reached by the cells cultivated in the bioreactor system: differentiation culture was performed at 5%O_2 with "differentiating" culture medium in static conditions (Figure 1).

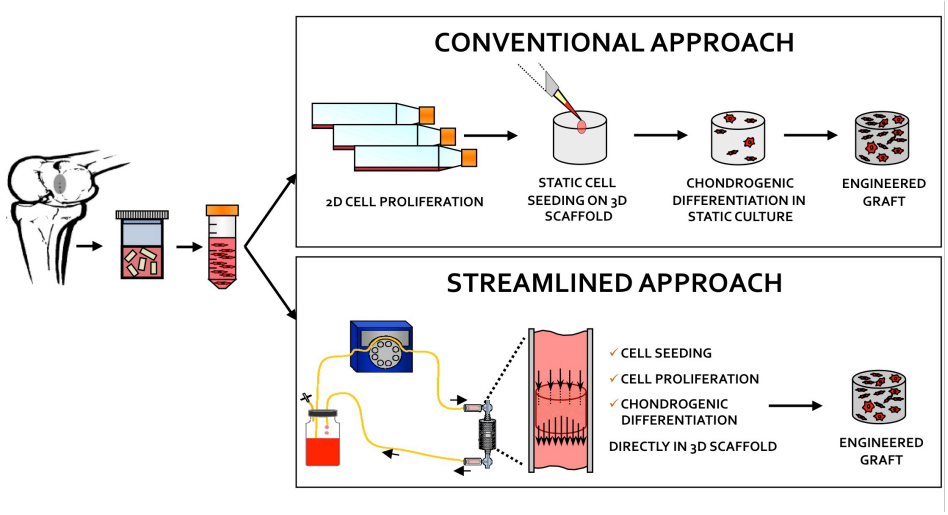

Figure 1 Tissue engineering paradigms for cartilage graft generation. Conventional approach implies intensive manual labor procedures such as cell expansion on 2D plastic surfaces, cell seeding on 3D scaffolds and graft maturation under static conditions. Bioreactor based graft production aims at streamlining the process by performing cell seeding, cell proliferation and chondrogenic differentiation directly into 3D scaffolds and within a single closed system.

Constructs after chondrogenic differentiation phase were harvested for molecular biology, biochemistry, mechanical and histological and immunohistochemical analyses.

In vivo evaluation of construct development:

Constructs upon bioreactor culture (either after proliferation or differentiation phases) were implanted subcutaneously in nude mice and harvested respectively after either 6 and 8 weeks or after 8 weeks, in order to compare total culture time and total in vivo development. Constructs were analyzed for histology as followed.

Histological and immunohistochemical analyses:

Constructs were fixed in PFA 4%, embedded in paraffin and further analyzed histologically and immunohistochemically. Safranin-O staining was done to visualize glicosamminoglycans (GAG) distribution and collagen type II immunostaining was performed as previously described (Candrian,et al. 2008). Immunohistochemistry for Ki67 (AbCam) was performed as suggested by the manufacturer's instructions and counterstained with alcian blue/immunofluorescence.

Mechanical tests:

Independent samples were also assessed biomechanically by indentation tests as previously described (Santoro, et al. 2010).

Biochemical analyses:

Constructs were biochemically analyzed to quantify GAG content by means of 1,9-dimethylmethylene blue assay and to assess the number of cells present per sample (CyQUANT® Cell Proliferation Assay Kit) as previously described (Candrian, et al. 2008).

Molecular biology analysis:

RNA extraction, cDNA preparation and RT-PCR were performed from the samples as previously described (Candrian, et al. 2008). 18s was used as housekeeping gene to normalize the expression of the genes of interest, namely collagen type I (COLL I), collagen type II (COLL II), Sox-9 (Applied Biosystems), Ki-67 (Applied Biosystems).

Statistical analysis:

Data are presented as mean value +/- SD. t-test or non-parametric test (Mann-Whitney) were performed after checking normal distribution of the values (significant p-value < 0.05 or 0.001).

Results

Firstly we assessed HAC streamlined culture within 3D hyaluronan meshes, with the ultimate goal to engi-

neer cartilage grafts based on conditions relevant for Hyalograft-C production. We compared this novel bioreactor-based paradigm with the conventional cartilage tissue engineering approach (Figure 1): on one side, freshly isolated chondrocytes where expanded and further differentiate directly in 3D within a closed bioreactor system; on the other, proliferation was performed in 2D in tissue flasks while matrix deposition was induced upon scaffold seeding according to the indications of current and conventional clinical applications.

In the streamlined approach, HAC could be extensively expanded directly within Hyaff-11 meshes, coated or not coated with fibronectin. Chondrocytes expanded on fibronectin-coated Hyaff-11 proliferated to a greater extent than in uncoated scaffold controls during the initial time frame of the proliferation phase, and reached a plateau at day 14, while those of the control group proliferated slowly and steadily until reaching the same threshold at day 14 (data not shown). In particular (Figure 2A), seven days of 3D expansion directly within fibronectin coated Hyaff-11 meshes resulted in 3.9±0.6 cell doublings, and in 14 days reached 4.7±0.6 doublings (corresponding to 2.7E+06 total cells per scaffold; or 4.8E+07 cells/cm^3). This number could be referred to the data present in clinical reports reporting such cell density for scaffold seeding after monolayer expansion (Marcacci et al., 2007).

As a matter of fact, in some donor cases the same desirable number of cell doublings could only be obtained by prolonging the culture time until day 21 (data not shown): nevertheless, the delay in switching to differentiation phase was experienced also in monolayer expanded cells, rising the problem of donor variability in proliferation capacity and the need of monitor and control of these culture parameters, that can be accomplished with bioreactor systems by means of oxygen sensors, as recently implemented in our systems (Santoro et al., submitted 2011).

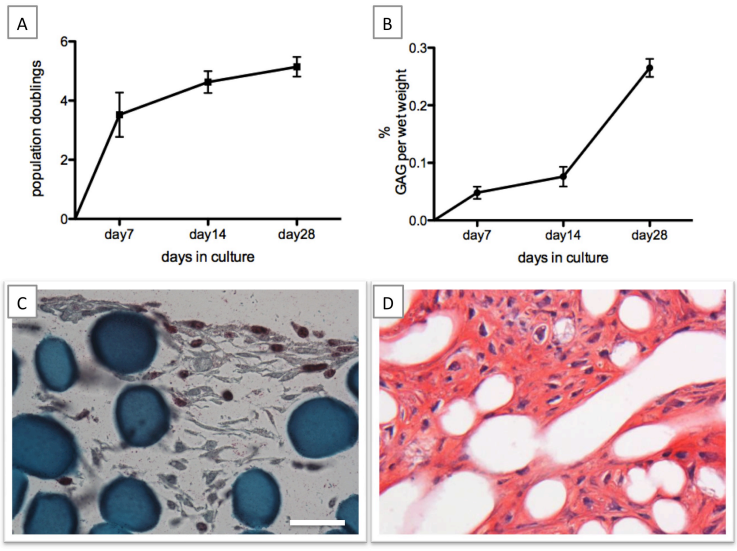

Figure 2 Bioreactor based approach in the context of Hyalograft-C graft generation. A) Trend of total population doublings along proliferation (day7, day14) and differentiation (day 28) phases in 3D scaffolds. B) trend of GAG production expressed as percentage of total scaffold wet weight along proliferation and differentiation phases. C) Immunohistochemistry at the end of proliferation phase (day 14) for proliferaitive marker Ki67 (red) with Alcian Blue as counterstaining (light blue). D) Safranin-O staining at the end of chondrogenic differentaition phase for GAG detection (red). Scale bar = 50um

As depicted in Figure 2C, the expression of the key marker for proliferation (Ki67) was detected via immunohistochemistry demonstrating that freshly isolated HAC were able to re-enter the cell cycle upon the quiescence they experience in the native microenviron-

ment. Subsequent to 3D proliferation phase, when cultured under differentiating conditions for two weeks, HAC stopped to proliferate (additional 0.6 doublings) and began to redifferentiate. Constructs cultured under this expansion/differentiation regime contained 0.25±0.05% GAG (Figure 2B) per wet weight and stained positive for Safranin-O staining (Figure 2D), similar to constructs generated in the same overall time frame by conventional manual culture processes (Candrian et al. 2008).

Once assessed the feasibility of the procedure relevant for the clinical scenario and the graft size of Hyalograft-C, we verified whether the streamlined approach described above could be further extended and applied to the generation of larger-scale cartilage grafts for uni-compartmental resurfacing (i.e., 50mm diameter x 4mm). The initial cell seeding number was determined by taking into account the same average biopsy size and digestion yield of the cartilage biopsy, but ultimately re-calculated to consider the larger graft dimensions, and thus, permitting a significantly lower cell seeding density (only 1.7E+05 cells/cm^3). The primary chondrocytes could be seeded and extensively expanded within the Hyaff-11 meshes, and depending on the donor, underwent 4.5 doublings in either 14 or 21 days, reaching cell densities of 8E+07 cells/cm^3. Interestingly, HAC seeded at lower cell density continued to proliferate even after the switch towards the chondro-

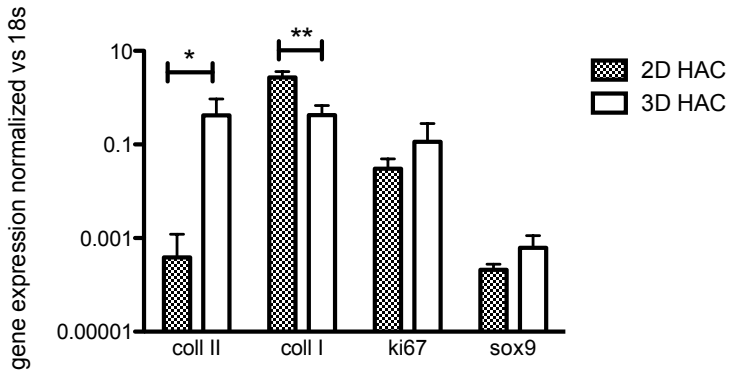

Figure 3 *Gene expression analysis for HAC expanded in monolayer (2D) and directly throughout 3D scaffolds within the bioreactor system. Data are normalized versus housekeeping gene 18s (* p<0.05; **p<0.01).*

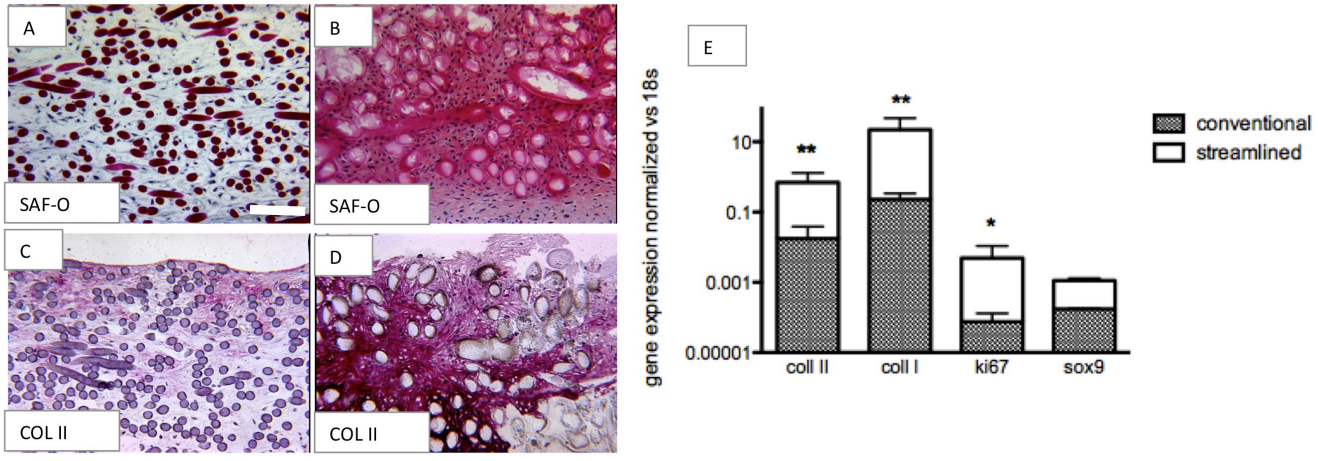

Figure 4 *Safranin-O staining (A,B) and collagen type II immunostaining (C,D) for conventional (A,C) and streamlined (B,D) approaches (Scale bar 200 um). Gene expression analysis for constructs generated with conventional and streamlined apporaches (E). Data are normalized versus housekeeping gene 18s (* p<0.05; **p<0.01).*

genic differentiation phase and they underwent further doublings in the last 2 weeks of the culture time.

Along proliferation phase, we performed a broader gene expression profile analysis in order to better describe the differences between 2D and 3D expanded cells: the results indicate up-regulation of proliferative marker (Ki-67), matrix related protein (COLL II) and the chondrogenic related marker SOX-9 and down regulation of COLL I compared to 2D expanded cells (Figure 3).

Upon chondrogenic differentiation phase, constructs were evaluated for matrix production by 3D expandedHAC: safranin-O staining (Figure 4B) was more pronounced as well as collagen type II expression (Figure 4D) if streamlined production was performed as opposed to conventional technique (Figure 4A,C). These data were confirmed also by molecular biology analysis for matrix molecule expression (collagen type I and collagen type II) (Figure 4E) and by GAG quantification.

Importantly, mechanical properties of the constructs were determined by indentation tests: the compression stress was measured as 0.11±0.07 MPa, which corresponds to 1.5% of the loading bearing capacity of native cartilage.

Finally, constructs were implanted subcutaneously in nude mice for 6-8 weeks in order to verify the stability and the quality of the engineered cartilage. Constructs processed in bioreactor units only for the 2 weeks (Figure 5A) did not rescue, during in vivo development, the production of matrix that was anticipated in the samples cultivated for further two weeks in bioreactor culture (Figure 5B). Importantly, engineered matrix obtained in vitro in these samples was stable upon in vivo incubation time., as depicted by the lack of macroscopic signs of hyperthrophy.

Discussion

The approach we described merges two different cell culture processes (i.e., cell proliferation and chondrogenic differentiation) directly in 3D scaffolds and within a single closed bioreactor unit, thus representing a significant step towards the development of a simplified and streamlined manufacturing process for chondral and endochondral graft production.

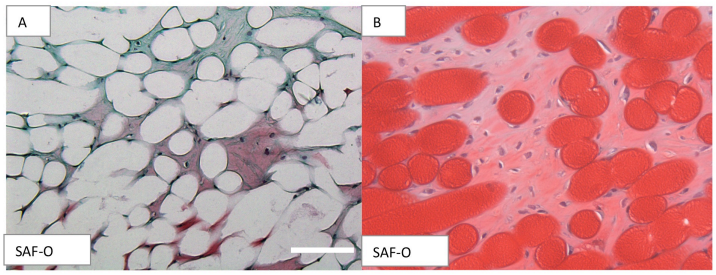

Figure 5 *Safranin-O staining for constructs precultiveted in vitro for two weeks (A) and 4 weeks (B) after in vivo culture (8weeks). (Scale bar 100um)*

Bioreactor system has been introduced to specifically implement singular culture phases, namely cell seeding, cell proliferation and tissue development; to decrease intensive manual procedures, thus risks of contamination and operator dependence variability, which are bottle necks factors for conventional labor techniques; and, additionally, to work as standalone closed unit where graft generation could be totally performed (Wendt et al., 2009).

From the clinical standpoint, we have demonstrated the feasibility in dealing with clinically relevant seeding densities and we have validated the approach with critically sized grafts. This novel strategy might allow the application of tissue engineering paradigms to large cartilage defect repair, which still represents one of the major concerns for clinical use of engineered products.

Starting from a low initial cell density, clinically relevant for the production of cartilage grafts in the size of FAB's Hyalograft-C, primary human chondrocytes could be extensively expanded directly within the Hyaff-11 meshes, reaching cell densities of 5E+07 cells/cm^3. For comparison, in the established procedure to manufacture Hyalograft-C, 3D constructs are cultured following cell seeding with a minimum of 5E+06 cells/cm^3 chondrocytes, which have previously been expanded for 14-21 days by extensive 2D monolayer culture (Marcacci et al., 2007). Therefore, in the same timeframe, it would be feasible to achieve similar or even higher cell densities through the 3D expansion method as compared to 2D monolayer culture.

Interestingly, while the scaffold coating did not appear to significantly increase the extent of proliferation (total cell doublings) at the two-week time point, fibronectin coating could potentially be used to increase the initial proliferation rate and ultimately reduce the time required for a proliferation phase.

When starting from an extremely low initial cell density, clinically relevant for the production of the large-scale cartilage grafts, primary human chondrocytes could be still extensively expanded directly within the Hyaff-11 meshes, sufficiently reaching FAB's current minimum cell density manufacturing specifications.

Furthermore, 3D expansion showed to support cell proliferation while maintaining the chondrogenic potential. In fact, cells expressed higher level of Ki-67, SOX9, and COLLII compared to 2D expanded cells. These data confirmed how 3D environment could influence the degree of dedifferentiation, the lost of the chondrogenic phenotype occurring when chondrocytes proliferate in monolayer.

As far as chondrogenic differentiation is concerned, 3D expanded cells could switch phenotype and produce at increasing extent cartilaginous matrix rich in GAG and collagens, in comparison with samples treated with the conventional procedure.

The bioreactor-based approach supported the generation of cartilaginous grafts, which were comparable in quality as those generated by long-established but labor intensive manual procedures (Candrian et al., 2008).

In vivo development of the constructs was followed for total of 8 weeks in ectopic mouse model: the boost with chondrogenic differentiation performed after proliferation phase resulted necessary to achieve good matrix deposition, thus stability and further maturation of the graft in vivo (Moretti et al., 2005). Interestingly, chondrocytes maintained the chondrogenic phenotype without undergoing any hyperthrophy that typically would occur using MSCs primed towards chondrogenic differentiation.

The culture system we optimized might accomplish the clinical demand of simplified tissue engineering approaches for small and large cartilage defects and may help in better understanding scientific relevant questions, such as dedifferentiation, maturation and phenotypical stability of articular chondrocytes, as essential events taking place during embryological limb developmental and cartilage-bone healing process.

Ultimately, the introduction of streamlined paradigm and development of GMP compliant bioreactor system might pave the way to the translation “bench to bed-side” for cartilage tissue engineering approaches (Martin, Smith and Wendt 2009).

References

Braccini A, et al. "Three-dimensional perfusion culture of human bone marrow cells and generation of osteoinductive grafts." Stem Cells 23, no. 8 (2005): 1066-72.

Brittberg M, et al. "Treatment of deep cartilage defects in the knee with autologous chondrocyte transplantation." N Engl J Med. 6, no.331 (1994): 889-95.

Brittberg M. "Autologous chondrocyte transplantation." Clin Orthop Relat Res., no. 367 (1999): S147-55. Candrian C, et al. "Engineered cartilage generated by nasal chondrocytes is responsive to physical forces resembling joint loading." Arthritis and Rheumatism 58, no. 1 (2008): 197-208.

Jakob M, et al. "Enzymatic digestion of adutlhuman cartilage yields a small fraction of the total available cells." Connect Tissue Reseach 44, no. 3-4 (2003): 173-80.

Lenas P, Moos M, and Luyten FP. "Developmental Engineering: A New Paradigm for the Design and Manufacturing of Cell-Based Products. Part I: From Three-Dimensional Cell Growth to Biomimetics of In Vivo Development." Tissue engineering Part B 15, no. 4 (2009): 381-394.

Marcacci M, et al. "Cell-based cartilage repair using the Hyalograft transplant." Cartialge repair strategies 13 (2007): 207-18.

Martin I, Smith T, and Wendt D. "Bioreactor-based roadmap for the translation of tissue engineering strategies into clinical products" Trends in Biotechnology 27, no. 9 (2009): 495-502.

Moretti M, et al. "Effects of in Vitro Preculture on in Vivo Development of Human Engineered Cartilage in an Ectopic Model." Tissue Engineering 11, no. 9/10 (2005): 1421-8.

Pelttari K, Wixmerten A, and Martin I. "Do we really need cartilage tissue engineering?" Swiss Med Wkly 139, no. 41-42 (2009): 602-609.

Santoro R, et al. "Bioreactor based engineering of large-scale human cartilage grafts for joint resurfacing." Biomaterials. 31 (2010): 8946-52.

Santoro R, et al. "Online monitoring of oxygen as a non-destructive method to quantify cells in engineered constructs." Submitted JTERM (2011).

Scherberich A, et al. "Three dimensional perfusion culture of human adipose tissue-derived endothelial and osteoblastic progenitors generates osteogenic constructs with intrinsic vascularization capacity." Stem cells 25, no. 7 (2007): 1823-9.

Stroebel S, et al. "Anabolic and catabolic responses of human articular chondrocytes to varying oxygen percentages." Arthritis Res Ther. 12, no. 2 (2010) Epub 2010 Mar 2.

Wendt D, et al. "Uniform tissues engineered by seeding and culturing cells in 3D scaffolds under perfusion at defined oxygen tensions." Biorheology 43, no. 3-4 (2006): 481-8.

Wendt D, Riboldi SA, Cioffi M, Martin I. "Potential and bottlenecks of bioreactors in 3D cell culture and tissue manufacturing." Adv Mater. 4, no. 21 (2009): 3352-67.

Chapter III

Model System To Control Cell Condensation Directly In 3D Scaffold In Bioreactor System

"The influence of the scaffold design on the distribution of adhering cells after perfusion cell seeding"

Enclosed is the pdf-file of the Paper published in Biomaterials, 2011 Apr; 32(11): 2878-84.

Biomaterials 32 (2011) 2878–2884

Contents lists available at ScienceDirect

Biomaterials

journal homepage: www.elsevier.com/locate/biomaterials

The influence of the scaffold design on the distribution of adhering cells after perfusion cell seeding

Ferry P.W. Melchels [a,1], Beatrice Tonnarelli [b,1], Andy L. Olivares [c], Ivan Martin [b], Damien Lacroix [c], Jan Feijen [a], David J. Wendt [b], Dirk W. Grijpma [a,d,*]

[a] MIRA Institute for Biomedical Technology and Technical Medicine, Department of Polymer Chemistry and Biomaterials, University of Twente, P.O. Box 217, 7500 AE, Enschede, The Netherlands
[b] Departments of Surgery and of Biomedicine, University Hospital Basel, Hebelstrasse 20, 4031 Basel, Switzerland
[c] Institute for Bioengineering of Catalonia (IBEC), Baldiri Reixac 4, 08028 Barcelona, Spain
[d] Department of Biomedical Engineering, University Medical Centre Groningen and University of Groningen, P.O. Box 196, 9700 AD Groningen, The Netherlands

ARTICLE INFO

Article history:
Received 29 October 2010
Accepted 8 January 2011
Available online 1 February 2011

Keywords:
Scaffolds
Microstructure
Cell adhesion
Confocal microscopy
Image analysis
Computational fluid dynamics

ABSTRACT

In natural tissues, the extracellular matrix composition, cell density and physiological properties are often non-homogeneous. Here we describe a model system, in which the distribution of cells throughout tissue engineering scaffolds after perfusion seeding can be influenced by the pore architecture of the scaffold. Two scaffold types, both with gyroid pore architectures, were designed and built by stereolithography: one with isotropic pore size (412 ± 13 μm) and porosity (62 ± 1%), and another with a gradient in pore size (250–500 μm) and porosity (35%–85%). Computational fluid flow modelling showed a uniform distribution of flow velocities and wall shear rates (15–24 s^{-1}) for the isotropic architecture, and a gradient in the distribution of flow velocities and wall shear rates (12–38 s^{-1}) for the other architecture. The distribution of cells throughout perfusion-seeded scaffolds was visualised by confocal microscopy. The highest densities of cells correlated with regions of the scaffolds where the pores were larger, and the fluid velocities and wall shear rates were the highest. Under the applied perfusion conditions, cell deposition is mainly determined by local wall shear stress, which, in turn, is strongly influenced by the architecture of the pore network of the scaffold.

1. Introduction

Zonal variations in extracellular matrix composition, as well as in cell distribution, have been observed in native tissues like articular cartilage, meniscal- and osteochondral tissue. Tissue grafts engineered in vitro to possess anisotropic properties that mimic the complex in vivo organisation could lead to better tissue function, regeneration, and integration as compared to homogenous grafts.

Bi-zonal engineered tissues, with locally varying composition and structure, have been generated in bioreactors inducing hydrodynamic flow [1], however, little is known about the specific effects of fluid flow on cell behaviour. Computational models have been developed, based on micro-computed tomography (μCT) reconstructions of the scaffold pore networks, to assess the influence of the scaffold micro-architecture on local shear stress profiles within the scaffold pores [2]. However, the irregular and random pore structures of most 3D scaffolds present significant challenges when attempting to correlate computational data to experimental observations in specific regions of the scaffold. As an alternative, scaffolds fabricated by solid freeform fabrication techniques, such as stereolithography, can be produced to posses highly regular and well-defined pore architectures [3], allowing the establishment of relations between local field variables calculated for the fluid dynamic field and the cellular behaviour within the 3D construct as a function of spatial location.

It was previously demonstrated that the perfusion of a cell suspension directly through the pores of a scaffold with a random pore structure resulted in a highly uniform distribution of cells [4]. The initial homogeneous cell distribution established a template for spatially uniform extracellular matrix deposition during subsequent perfusion culture in the bioreactor system [5]. With the ultimate goal of engineering biomimetic zonal tissue grafts, in this work, we hypothesised that gradients in shear rate, induced by anisotropic gradient scaffold architectures, would modulate the cell distribution during perfusion cell seeding.

* Corresponding author. MIRA Institute for Biomedical Technology and Technical Medicine, and Department of Polymer Chemistry and Biomaterials, University of Twente, P.O. Box 217, 7500 AE, Enschede, The Netherlands. Tel.: +31 53 489 2966; fax: +31 53 489 2155.
E-mail address: d.w.grijpma@tnw.utwente.nl (D.W. Grijpma).
[1] Equally contributing authors.

0142-9612/$ – see front matter © 2011 Elsevier Ltd. All rights reserved.
doi:10.1016/j.biomaterials.2011.01.023

2. Experimental

2.1. Scaffolds

Photo-polymerisable poly(D,L-lactide) (PDLLA) macromers were synthesised in a similar way as previously described [6]. In short, linear hydroxy-terminated oligomers with a molecular weight of 1.2 kg/mol were synthesised by ring opening polymerisation, followed by a reaction for 9 h with methacrylic anhydride (Sigma–Aldrich, 50% molar excess) at 110 °C in the presence of 0.15% α-tocopherol inhibitor (vitamin E, Fluka) to prevent preliminary crosslinking. The excess methacrylic anhydride and the formed methacrylic acid were removed by vacuum distillation (residues 0.7 and 0.4 wt%, respectively). The macromers were used to formulate a stereolithography resin further comprising 18 wt% dry N-methylpyrrolidone (NMP, Fluka) as a non-reactive diluent, 3.6 wt% ethyl-2,4,6-trimethylbenzoylphenyl-phosphinate (Lucirin TPO-L photo-initiator from BASF) and 0.15 wt% Orasol Orange G dye (Ciba SC).

Two scaffold designs were developed using K3DSurf v0.6.2 software, both based on the gyroid architecture [3,6]. The first design is an isotropic design (type I) with constant porosity throughout the (cylindrical) scaffold. Another scaffold (type G) was designed to have a porosity gradient in the radial direction, by making the offset value in the implicit function (see below) dependent on the scaffold radius. The following equations were used to describe the scaffold designs, both with boundary conditions $x^2 + y^2 < (10\pi)^2$ and $|z| < 5\pi$:

$$I : \cos(x)\sin(y) + \cos(y)\sin(z) + \cos(z)\sin(x) - 0.15 = 0$$

$$G : \cos(x)\sin(y) + \cos(y)\sin(z) + \cos(z)\sin(x) + 0.0015\left(x^2 + y^2\right) - 0.90 = 0$$

Cylindrical scaffolds (diameter 8 mm, height 4 mm) were fabricated from CAD designs using an EnvisionTec Perfactory Mini Multilens stereolithography apparatus, and post-treated as previously described [6]. Micro computed tomography (μCT, GE eXplore Locus SP operated at 80 kV, 80 μA and 15 μm resolution without filter) was used for structural analyses of the fabricated scaffolds and to obtain digital meshes as input for flow analyses (MicroView software).

2.2. Fluid flow modelling

The flow of fluid (medium) through the pore networks of both scaffold types was modelled using a computational fluid dynamics approach, and taking the geometry of the bioreactor chamber into account. With μCT iso-surface meshes as input, volumetric fluid meshes were made using Mimics software (Materialise) to obtain a total of 2,375,010 tetrahedral elements for the type I scaffold and 2,253,778 elements for the type G scaffold. The boundary conditions used in modelling the perfusion were in correspondence with the perfusion cell seeding experiment (see below). No-slip surface conditions and zero outlet pressures were assumed. In the model, the material from which the scaffolds were prepared was rigid and impermeable. Profiles of fluid flow velocity, fluid shear rates and fluid shear stresses were calculated using Fluent 6.3 (Ansys) software. The fluid was modelled using the viscosity ($\eta = 1.45 \cdot 10^{-3}$ Pa·s) and density ($\rho = 1000$ kg·m^{-3}) of Dulbecco's modified eagle medium (DMEM, both at 37 °C).

2.3. Perfusion cell seeding

The scaffolds were perfusion seeded with expanded human articular chondrocytes (HAC) in separate bioreactors as previously described [4]. Scaffolds were lightly press-fit and clamped within a bioreactor chamber such that the fluid was forced to flow through its pores. Then, 3 million HAC suspended in 8 mL media per chamber were dynamically seeded for 16 h at an inlet velocity of 1 mm/s. Following perfusion seeding (3 specimens per scaffold architecture), cells were stained with SYTO-13 green fluorescent dye (Molecular Probes) to assess the distribution of live cells within the scaffolds. Confocal microscopy images were taken using a confocal laser scanning microscope (CLSM, 7500-Zeiss) with a 10× objective and the aperture set at 1 Airy unit (this corresponds to an image depth of 10 μm). Entire scaffold cross-sections were imaged by scanning over adjacent blocks of z-stacks, up to 500 μm in depth. The confocal microscopy images were thresholded to black-and-white and subsequently used to determine relative cell densities. Relative cell densities were expressed as the relative area of the image covered with cells (the fraction of black pixels). To obtain quantitative distributions as a function of the scaffold radius, the coordinates of each scaffold centre were first determined. The images were then partitioned in equidistant rings from the centre towards the periphery with radius increments of 100 μm. The cell density in each concentric ring was determined, as the percentage of the area covered with cells. The quantitative results of the cell distributions are averaged over at least 21 confocal images per each analysed sample.

The polar moments of inertia for wall shear rate and cell density were calculated using:

$$J = \iint r^2 \rho(\vec{r}) dA = \sum_i^N r_i^2 \rho_i \pi \left(r_i^2 - r_{i-1}^2\right)$$

where r is the distance from the scaffold centre, ρ is the density function of either the local average wall shear rate or the cell density, and $dA = \pi(r_i^2 - r_{i-1}^2)$ is the area for each equidistant ring.

3. Results

3.1. Scaffolds

Poly(D,L-lactide) macromers were successfully synthesised, the degree of functionalisation of the end groups was more than 95%. After mixing with diluent, photo-initiator and dye, the PDLLA resin was used to build the designed scaffolds by stereolithography. After extraction and drying, the built scaffolds were visualised by μCT imaging. Fig. 1 shows that the scaffold designs were very accurately reproduced. The porosity gradients in the built type G scaffolds can be clearly seen.

For both scaffold types, Fig. 2 shows the distribution of local porosity values as a function of distance from the scaffold central axis. Data from the computer designs as well as from the μCT analyses are presented. The porosity gradient in the type G scaffold leads to a gradient in pore size as well; sizes range from approximately 500 μm in the centre of the scaffold to 250 μm at the periphery.

The type I scaffold shows low variance in porosity and pore size. An overall porosity of 62 ± 1% was determined, with an average pore size of 412 ± 13 μm. For the type I scaffold in particular, the periodicity of the trigonometric functions is reflected by the regular oscillations in the determined local porosity values from the centre of the scaffold outwards. Although in the case of this scaffold type an isotropic porosity of 55% was designed, the μCT data show that the local porosity increases from the centre of the scaffold outwards towards its perimeter. This is the result of overcure, a phenomenon that can occur in the fabrication of porous structures by stereolithography [6]. In the type G scaffold, the effect of overcure is minimal because of the high porosity values in the central region of the scaffold.

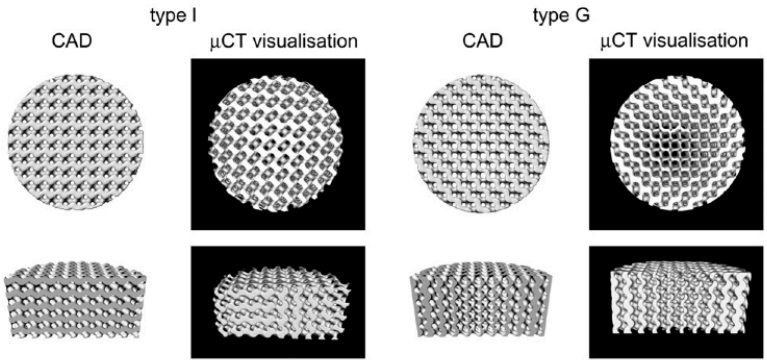

Fig. 1. Top row: top-view images of type I (isotropic design) and type G (gradient design) gyroid scaffolds comparing the computer-aided designs (CAD) with μCT-visualisations of the built structures. Bottom row: cross-sections, clearly showing the gradient in porosity and pore size in the type G scaffold. The diameter of the scaffolds is 8 mm.

3.2. Fluid flow modelling

The flow of fluid through both scaffold architectures was modelled using a computational fluid dynamics approach. To represent the scaffold pore architectures, data from the μCT analyses of the built structures (and not those of the computer designs) were used. The modelling, in which the geometry of the perfusion bioreactor chamber was taken into account as well, resulted in the velocity profiles depicted in Fig. 3. Here, the values of the local fluid velocities are shown as coloured vectors. The characteristic zero mean-curvature of the gyroid pore network architecture implies the absence of flow-disturbing elements. In the given perfusion regime, this results in laminar fluid flows (the maximum calculated Reynolds number is 0.12). Average fluid flow velocities are 0.86 mm/s for both scaffold types. Parabolic fluid velocity profiles develop in each of the channels that run through the scaffolds; the local velocity is highest in the centre of the channel. The modelling shows, that in the type I scaffold the flow profile is quite uniform with maximum velocities of approximately 2.8 mm/s. In the type G scaffold undisturbed laminar flows are also observed, but the radial gradient in porosity leads to a clear gradient in fluid flow velocities. For this scaffold architecture the maximum velocities in the central part of the scaffold are close to 4.0 mm/s, while they strongly decrease to near zero at the periphery. The (direction of the) observed gradient in flow velocities is due to the lower resistance of the larger-diameter channels.

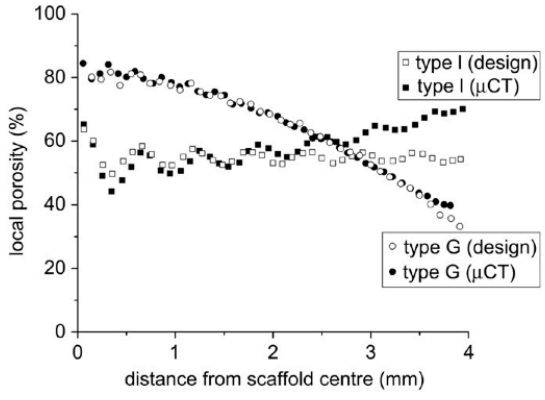

Fig. 2. Local porosity as a function of the distance from the central axis of the scaffold, for cylindrical type I (isotropic) and type G (gradient) scaffolds. The data from the μCT analyses (average of 2 samples each) are compared to the computer-aided designs. Local porosity values are determined at 100 μm intervals.

At the scaffold wall the velocity of the fluid is zero, and wall shear rates are best used to describe the velocity with which suspended cells flow past the surface of the pores. Wall shear rate is defined as the slope of the velocity profile at the fluid–wall interface:. The lower part in Fig. 3 shows 3D views of the scaffolds, where part of the scaffolds is coloured to indicate the distribution of local wall shear rate values. Here, the uniformity of the fluid velocity profile in scaffold type I is also reflected in rather uniform wall shear rates throughout the structure. In contrast, scaffold type G shows considerably reduced wall shear rates towards the periphery of the scaffold when compared to wall shear rates in the centre.

The wall shear rate not only determines the velocity of the passing cell suspension, but it also determines the hydrodynamic force that adhering cells are exposed to. This force can be expressed per unit of area as the wall shear stress (in Pa), and is the product of the wall shear rate and the kinematic viscosity of the fluid medium. The wall shear stress is therefore an important parameter in cell adhesion processes [7]. The average wall shear stresses in scaffold types I and G are 31 and 27 mPa, respectively, and range from near-zero values to maximum local values of approximately 65 mPa. The effects of flow-induced shear stress on cell adhesion have been studied extensively [8,9,10]. The critical shear stress for cell detachment to occur depends on the material on which the cells are cultured, but has been found to range between 1 and 3 Pa [11,12,13]. For the range of wall shear stress values occurring in our perfusion setup, flow-induced cell detachment will not occur.

3.3. Assessment of cell distributions

Upon perfusion seeding, stained constructs were analysed by confocal microscopy. Imaging of the cells and the cell distribution by confocal microscopy and modelling the fluid flow during perfusion cell seeding, allows comparing the spatial density of adhering seeded cell with spatial fluid flow conditions. The example in Fig. 4 shows a cross-section of a type I scaffold (10 μm confocal thickness) where we can distinguish individual cells adhering to the scaffold surface (see insert). The right part of the figure shows the modelled wall shear rate profile in a cross-section. The insert shows that at a small size scale (within a pore), the shear rates range between 0 and 30 s^{-1}. The macroscopic distribution of shear rates, however, is homogeneous; only little differences in shear rate values are observed when comparing unit cells from the central part of the scaffold to those at the periphery.

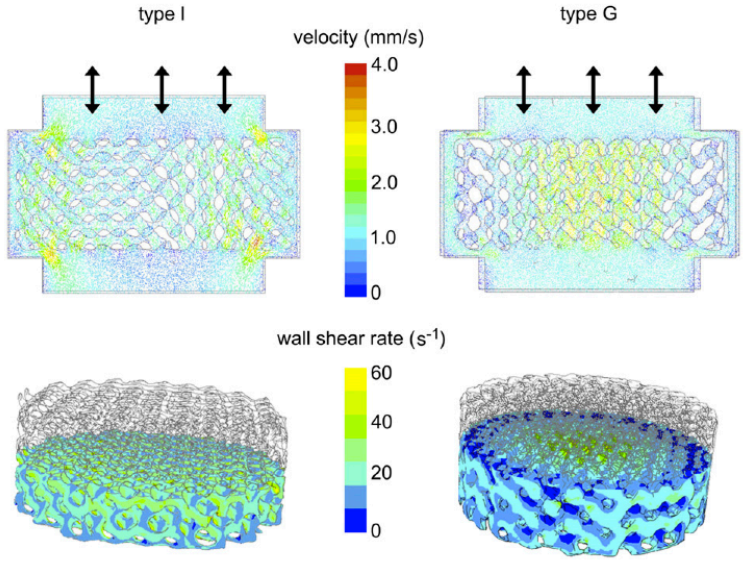

Fig. 3. Fluid flow velocity- and wall shear rate profiles for scaffold types I (isotropic) and G (gradient). The velocity vectors between two parallel sections (at a distance of 0.5 mm) in the direction of the flow path are shown. The diameter of the scaffolds is 8 mm. The spots with high local velocities at the scaffold edges (inlet and outlet) are artefacts.

Fig. 5 depicts thresholded confocal microscopy images of both scaffold types. The cell densities in confocal microscopy images will depend on the surface area available for cell adhesion. For both scaffold types a surface area of $1.2 \cdot 10^3$ mm^2 was determined by μCT, corresponding to an overall specific surface area of 4.8 mm^{-1}. As a result of the well-defined and repetitive nature of the pore network architectures, the local values for the specific surface area (distribution of surface area throughout the scaffold) show only minimal fluctuation. It is therefore possible to compare the observed cell densities in different regions of both scaffold types.

The top left image in Fig. 5 shows a very homogeneous distribution of cells after seeding of the type I scaffold, determined, by inducing uniform velocity- and wall shear rate profiles of the flowing cell suspension. For the type G scaffold, with a radial gradient on pore size and porosity, an anisotropic distribution of cells is observed after perfusion cell seeding. The top right image in Fig. 5 shows that the cell density is markedly higher in the centre of the scaffold than at the periphery.

The distribution of adherent cells was quantified by determining the cell density as a function of the distance in radial direction from the scaffold centre. Fig. 6 depicts the radial distribution of cell densities as histograms, determined from the thresholded images of the cell densities on the different scaffolds such as shown in Fig. 5. Here, the presented values are an average of at least 9 subsets from 3 different scaffolds, each of 70 μm thickness. The values are normalised for each image to enable direct comparison of the relative cell distributions. Besides the radial cell distributions, the corresponding modelled local average wall shear rates are shown.

For the isotropic scaffold (type I), a uniform distribution in the cell density and in the modelled average wall shear rate can be observed. The average wall shear rate values are scattered over a relatively small range of 16–24 s^{-1}, and the values show no relation with location in the scaffold or cell density. The regular isotropic architecture of the scaffold leads to a uniform distribution of flow and results in very homogeneously seeded scaffolds.

In the gradient type G scaffold however, we clearly see anisotropic distributions of seeded cell densities and wall shear rates. Both the cell density and the wall shear rate are high in the centre of the scaffold and much lower at the periphery. The polar moments of inertia give a quantitative measure of how much a radial distribution is spread outwards. For the average wall shear rate the type G scaffold has a value of $6.4.10^3$ s^{-1} whereas the type I scaffold has a value of $8.4.10^3$ s^{-1}. For the relative cell density these values are $3.0.10^2$ and $6.6.10^2$ respectively. As far as the gradient scaffold is concerned, the correlation between the cell density and the modelled average wall shear rate is clearly visualised in the bottom right image of Fig. 6. It is apparent that the highest cell densities in the seeded scaffolds are observed in regions were the wall shear rate of the fluid flow was highest.

4. Discussion

Under flow conditions, the deposition rate of suspended particles on a surface depends on many parameters such as advective transport and diffusivity [14], colloidal interactions [15], concentrations of ligands and receptors [16], binding strengths and bond-forming kinetics [17] and available surface area [18]. Because of the well-defined scaffold architectures and the constant perfusion conditions, many of these parameters do not vary throughout the scaffolds in our perfusion seeding experiments. We can therefore directly assess how flow parameters affect the final distribution of cells upon bioreactor seeding throughout scaffolds with different geometries.

When looking solely at cell–material interactions under fluid flow, it seems contradictory that areas of highest shear and fluid velocity would have higher cell numbers. From this it follows that the relative cell densities resulting from perfusion seeding depend more on the delivery of cells to the different regions of the scaffold than on the kinetics of the cell attachment process that follows, as in the employed shear stress regime no cell detachment can be expected. As in our experiments the flow is laminar, the suspended cells will follow the flow profile (like tracer particles), with minimal advective transport in directions perpendicular to the flow. Only cells close to the pore wall of the scaffold are likely to contact the

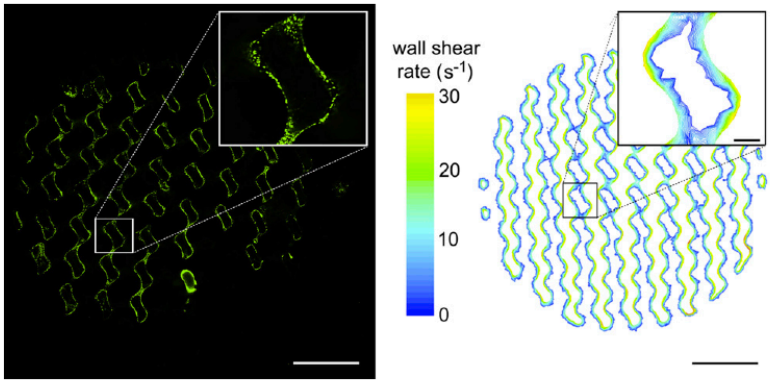

Fig. 4. Left: representative confocal microscopy image of a type I gyroid scaffold seeded with cells, showing the distribution of live adhering cells throughout a cross-section of the scaffold. Right: image of a similar cross-section, showing the modelled distribution wall shear rates of the fluid during perfusion cell seeding. Scale bars are 2 mm for the larger images and 200 μm for the inserts.

surface. As the wall shear rate is a measure of the velocity of the cell suspension close to the scaffold pore wall, it determines the number of cells that flow past the surface per unit of time. This correlation is clearly shown in the right parts of Fig. 6, where the highest cell numbers are close to the centre of the type G scaffold, where wall shear rates are highest.

From this, it follows that we can influence distributions of seeded cells in perfusion seeding by tailoring the architecture of the pore network of the scaffold. In well-defined isotropic gyroid architectures we can obtain very homogeneous distributions of adhering cells, while gradients in pore size and porosity lead to gradients in cell densities. The scaffold architecture affects the local fluid flow velocities of the cell suspension, the number of cell-scaffold contacts per time unit and, therefore, the local cell deposition rates. By preparing other scaffolds with designed architectures, other flow profiles and other cell distributions in the scaffolds may be obtained. Other cell

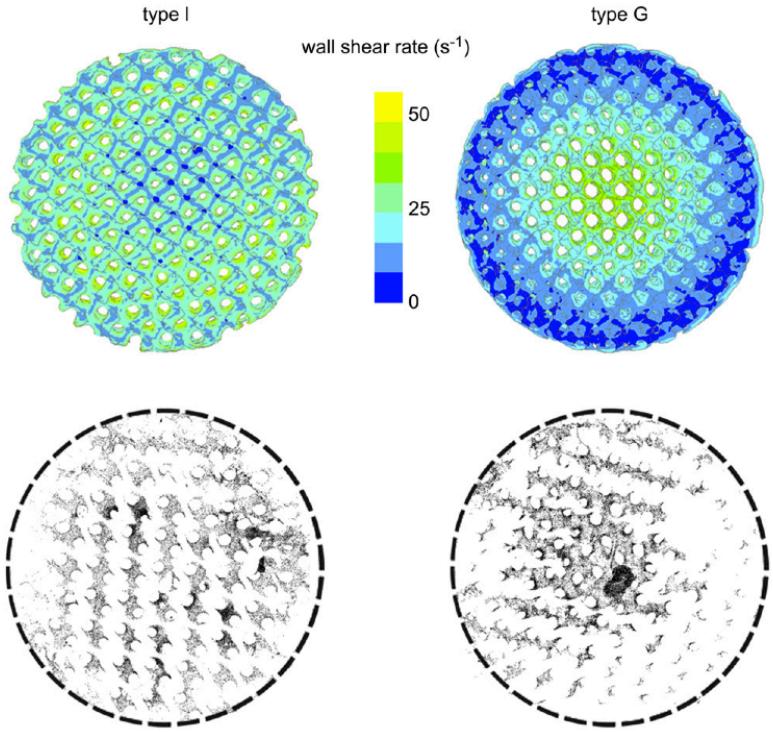

Fig. 5. Comparison of the distribution of cell densities and wall shear rates in cross-sections of type I (isotropic) and type G (gradient) scaffolds. Top: representative thresholded z-stacks of confocal microscopy images (500 μm thickness) showing adhering cells after perfusion seeding. Bottom: middle cross-sections of scaffolds showing wall shear rate distributions of the fluid during perfusion cell seeding.

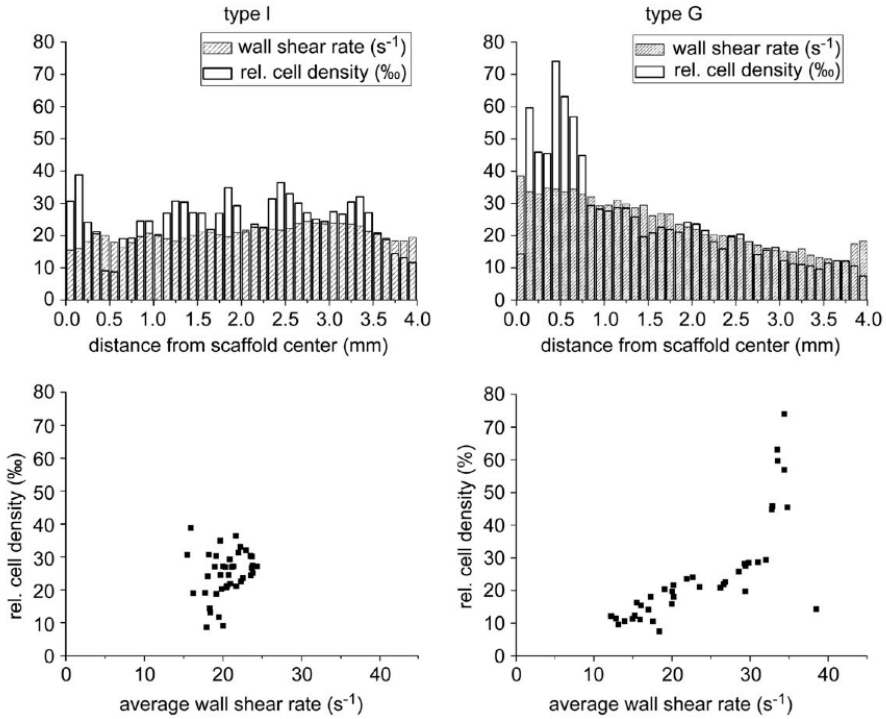

Fig. 6. Quantitative comparison of the distributions in modelled wall shear rate and measured cell density in cross-sections of the isotropic type I (left) and gradient type G (right) scaffolds. Top: distributions of local average wall shear rates (s^{-1}) and of cell densities as a function of the distance in the radial direction from the scaffold centre. Bottom: scatter plot of the cell density as a function of the modelled local average wall shear rate.

types may exhibit different seeding kinetics as these may have different types and densities of adhesion molecules. However, since the flow-induced transportation of cells towards the scaffold pore surface seems to be the determining factor in our setup, similar cell distributions may be expected using different cells and/or scaffold materials. Under the well-controlled conditions in the used perfusion bioreactor system –applying wall shear stresses that are well below values typical for cell detachment to occur- the internal scaffold pore architecture is the determining factor influencing the final cell distribution.

As we have studied only one time-point, the specific kinetics of the cell seeding process can not be derived from our data. For this, cell adhesion experiments using a flow displacement system should be performed as a function of time [19]. Shear rate-dependent adsorption rates can be determined in such experiments. The effect of the three-dimensional architecture of the porous structure could then be investigated separately, and better understanding and control of regional differences in cell deposition could be achieved. Furthermore, critical wall shear stress values could be determined at higher flow rates.

In this work we related averaged cell densities to averaged wall shear rates, as a function of distance from the scaffold central axis. A next step in the development of this model system would be to assess cell distributions at the pore level, since in each pore a range of wall shear rates exists. Such a model system would then enable to experimentally validate theories of mechano-regulation of cell behaviour. These theories are based on computational models, in which the probabilistic behaviour of cells resulting from mechanical stimuli acting at the cellular level is modelled. In this way, cell proliferation and differentiation and extracellular matrix formation could be predicted [20,21]. Particularly the ability to visualise individual cells and compute their local hydrodynamic environment provides an experimental framework to test, adjust and support these theories.

5. Conclusions

We have developed a model system to assess the influence of local fluid flow characteristics in designed porous scaffolding structures on the distribution of cells upon perfusion seeding. The density of adhering cells was correlated to the local average wall shear rate at the surface of the pore walls. While scaffolds with an isotropic gyroid pore network architecture show very homogeneous distributions of shear rates and cell seeding densities upon perfusion cell seeding, gyroid scaffolds prepared with gradients in pore size and porosity show anisotropic adherent cell densities. The highest cell densities in the scaffolds could be related to regions with larger pores, higher fluid flow velocities and higher wall shear rates. The ability to influence the distribution of seeded cells in a porous structure upon seeding will be fundamental to control the engineering of complex three-dimensional tissue constructs with defined structural organisations.

Acknowledgements

We acknowledge the European Union for their financial support (STEPS project, FP6-500465).

Appendix

Figures with essential colour discrimination. Certain figures in this article, particularly Figs. 3, 4, and 5, are difficult to interpret in black and white. The full colour images can be found in the on-line version, at doi:10.1016/j.biomaterials.2011.01.023.

References

[1] Marsano A, Wendt D, Raiteri R, Gottardi R, Stolz M, Wirz D, et al. Use of hydrodynamic forces to engineer cartilaginous tissues resembling the non-uniform structure and function of meniscus. Biomaterials 2006;27(35):5927–34.

[2] Cioffi M, Kuffer J, Strobel S, Dubini G, Martin I, Wendt D. Computational evaluation of oxygen and shear stress distributions in 3D perfusion culture systems: macro-scale and micro-structured models. J Biomech 2008;41(14):2918–25.

[3] Melchels FPW, Bertoldi K, Gabbrielli R, Velders AH, Feijen J, Grijpma DW. Mathematically defined tissue engineering scaffold architectures prepared by stereolithography. Biomaterials 2010;31:6909–16.

[4] Wendt D, Marsano A, Jakob M, Heberer M, Martin I. Oscillating perfusion of cell suspensions through three-dimensional scaffolds enhances cell seeding efficiency and uniformity. Biotechnol Bioeng 2003;84(2):205–14.

[5] Wendt D, Stroebel S, Jakob M, John GT, Martin I. Uniform tissues engineered by seeding and culturing cells in 3D scaffolds under perfusion at defined oxygen tensions. Biorheology 2006;43(3–4):481–8.

[6] Melchels FPW, Feijen J, Grijpma DW. A poly(D, L-lactide) resin for the preparation of tissue engineering scaffolds by stereolithography. Biomaterials 2009;30(23–24):3801–9.

[7] Morigi M, Zoja C, Figliuzzi M, Foppolo M, Micheletti G, Bontempelli M, et al. Fluid shear-stress modulates surface expression of adhesion molecules by endothelial-cells. Blood 1995;85(7):1696–703.

[8] Ando J, Yamamoto K. Vascular mechanobiology - endothelial cell responses to fluid shear stress. Circ J 2009;73(11):1983–92.

[9] Rosenman JE, Kempczinski RF, Pearce WH, Silberstein EB. Kinetics of endothelial-cell seeding. J Vasc Surg 1985;2(6):778–84.

[10] Feugier P, Black RA, Hunt JA, How TV. Attachment, morphology and adherence of human endothelial cells to vascular prosthesis materials under the action of shear stress. Biomaterials 2005;26(13):1457–66.

[11] Isenberg BC, Williams C, Tranquillo RT. Endothelialization and flow conditioning of fibrin-based media-equivalents. Ann Biomed Eng 2006;34(6):971–85.

[12] Macario DK, Entersz I, Abboud JP, Nackman GB. Inhibition of apoptosis prevents shear-induced detachment of endothelial cells. J Surg Res 2008;147(2):282–9.

[13] Smith RL, Donlon BS, Gupta MK, Mohtai M, Das P, Carter DR, et al. Effects of fluid-induced shear on articular chondrocyte morphology and metabolism in vitro. J Orthop Res 1995;13(6):824–31.

[14] Adamczyk Z, Vandeven TGM. Deposition of particles under external forces in laminar-flow through parallel-plate and cylindrical channels. J Colloid Interf Sci 1981;80(2):340–56.

[15] Sjollema J, Busscher HJ. Deposition of polystyrene latex-particles toward polymethylmethacrylate in a parallel plate flow cell. J Colloid Interf Sci 1989;132(2):382–94.

[16] Cozensroberts C, Quinn JA, Lauffenburger DA. Receptor-mediated adhesion phenomena - model studies with the radial-flow detachment assay. Biophys J 1990;58(1):107–25.

[17] Hammer DA, Lauffenburger DA. A dynamic-model for receptor-mediated cell-adhesion to surfaces. Biophys J 1987;52(3):475–87.

[18] Meinders JM, Busscher HJ. Adsorption and desorption of colloidal particles on glass in a parallel-plate flow chamber - influence of ionic-strength and shear rate. Colloid Polym Sci 1994;272(4):478–86.

[19] Busscher HJ, van der Mei HC. Microbial adhesion in flow displacement systems. Clin Microbiol Rev 2006;19(1):127–41.

[20] Sandino C, Checa S, Prendergast PJ, Lacroix D. Simulation of angiogenesis and cell differentiation in a CaP scaffold subjected to compressive strains using a lattice modeling approach. Biomaterials 2010;31(8):2446–52.

[21] Olivares AL, Marshal E, Planell JA, Lacroix D. Finite element study of scaffold architecture design and culture conditions for tissue engineering. Biomaterials 2009;30(30):6142–9.

Conclusions and final remarks

1. Summary: aims and results of the experimental work

This thesis dissertation is enclosed in the field of investigation aimed at implementing and streamlining skeletal tissue engineering approaches. Conventional manufacturing processes for graft generation have been recently challenged by new insights in basic biology, technological tools and clinical demands. Thus, we queried tissue engineering dogmas from all these different perspectives.

In **Chapter I**, we have described for the first time the capacity of expanded, adult human MSC to generate frank bone through endochondral route by engineering cartilaginous template in vitro. With this protocol, we aimed at exemplifying the paradigm of developmental engineering in the context of bone regeneration. In fact, the process recapitulated the time course of events occurring during limb development, namely (i) cellular condensation and hypertrophic chondrogenesis, (ii) morphogen signaling activation, (iii) formation of bony collar through perichondral ossification, (iv) matrix remodeling and vascularization, and (v) formation of complete bone organ, including hematopoietic elements.

Thus, with the perspective of clinical applications, we applied bioreactor technology to control, streamline and upscale the process.

Bioreactors could be considered a powerful tool to overcome conventional tissue manufacturing processes. As shown in **Chapter II**, bioreactor can be exploited as single closed system where all cell culture phases can be performed. We first focused on optimizing the first two events of the endochondral route (i.e. condensation and chondrogenic differentiation), which, as a matter of fact, represent the complete process of cartilage graft manufacturing. Therefore we hypothesised a clinical scenario for cartilage defect reconstruction, so that freshly isolated cells (at clinically relevant starting density) were first expanded directly throughout 3D scaffold and within the bioreactor system, and, secondly induced at generating a cartilaginous like graft. We succeeded in engineering a graft product that is comparable with the one obtained with conventional techniques and might fulfil quality release criteria for clinical application. We could develop a novel bioreactor based manufacturing paradigm for cartilaginous graft production, which could be applied for cartilage tissue engineering and used as platform for endochondral recapitulation.

Finally, as depicted in **Chapter III**, we wanted to achieve control over cell condensation, throughout 3D scaffold and under perfusion regime, optimizing the first step of bioreactor-based endochondral tissue engineering. Therefore we aimed at applying computational fluid dynamics model to predict cell behaviour within specific 5milieu and, more precisely, we generated a model system where scaffold design and computed perfusion regime were optimised and validated experimentally by using controlled cell distribution upon per-

fusion seeding as readout. Tuning scaffold porosity and, therefore, velocity and shear stress profile we could change cell distribution throughout the scaffold. These results highlight the paramount importance of bioreactor systems as tool to monitor and control culture parameters or entire manufacturing phases.

2. Relevance of the study and future perspectives

Nowadays, the success of tissue engineering may depend on overcoming current limitations related to identification of optimal cell type, tissue manufacturing process, feasibility of clinical translation. As a matter of fact, in the last years the necessity of tissue engineering has been questioned, in relation to cost-effectiveness, safety, compliance to GMP rules and potency of engineered products over existing medical therapies.

Developmental engineering paradigm and bioreactor technology have together the potential to remarkably innovate conventional regenerative medicine, from the conceptual and methodological standpoint. The combination of the recent progress in developmental biology as well as in bioreactor-based cell culture methods might provide the opportunity (i) to switch from trial-and-error approaches towards rational experimental design, (ii) to create model systems to test specific scientific hypotheses, (iii) to implement and standardize conventional tissue engineering, and (iv) to ultimately target clinical applications.

The modern notion that in vitro processes should recapitulate in vivo development and repair may offer an alternative strategy that intrinsically contribute to implementation by defining specific boundaries, such as optimal cell type and critical intermediate events along the manufacturing process.

In the first work we presented (**Chapter I**), endochondral route was recapitulated with adult MSC, specific progenitors for skeletal development and repair processes and clinically compliant cell source.

From the molecular standpoint, key morphogenetic cross-talks were established between early and late hypertrophic cells in our model system. However, spatial organization of the different cell populations was not exactly reproducing the pattern observed in the growth plate during development, impairing self-organization of the tissue. Thus, next challenges in this tissue engineering field would be to unravel the foundations of spatio-temporal evolution of the tissue: conquering the control of cellular interactions in 4D will be of paramount importance for basic research and for applied tissue engineering processes.

Moreover, orthotopic implantation in immunocompetent animal model could shed light on biomechanical and inflammatory/immune mechanisms that likely participate in endochondral process as well as in fracture healing. Further experiments targeting the role of host cells in bone forming process might pave the way to new generation of off-the-shelf grafts, properly instructive for events occurring upon implantation.

Our model was based on small-scale, scaffold-free constructs that would not be relevant in a clinical scenario. Further investigations are warranted for the clinical implementation of the developed paradigm. Scaling-up of the constructs would be the next step, possibly with the integration of the bioreactor system to allow in vitro simplified, streamlined and controlled culture.

With the attempt to ameliorate graft manufacturing process, bioreactors could be indeed considered a powerful tool to substitute conventional product pipelines. If control and standardization of products and manufacturing processes have been so far suboptimal and might have represented an obstacle for clinical application, bioreactors could target these weaknesses and further ameliorate the graft production. Bioreactors, as described in **Chapter II**, have been demonstrating their key role in improving seeding and culture conditions, in monitoring critical culture parameters, in providing single closed system where specific culture phases can be performed, in up-scaling graft and production for efficient clinical translation. Moreover, as depicted in **Chapter III,** bioreactors could be exploited as model systems where culture conditions (i.e. scaffold design and perfusion regime) are controlled and validated in relation to cell behaviour, in feed-back loop fashion: this kind of investigations may lead to a better understanding of the role of these key culture parameters.

Thus, bioreactor based approaches might pave the way for the warranted “bench to bed-side” translation for tissue engineering products and next experiments will be focusing on the generation of stand alone bioreactor systems to assure GMP compliance towards the clinical application of developmental engineering paradigms for skeletal regeneration.

Paradoxically, tissue engineering needs to identify new strategies that may go beyond tissue engineering itself. The recapitulation of biological and molecular events occurring during development in graft production pipeline might suggest to overcome the traditionally envisaged implantation of preformed and mature grafts and to approach a more modern perspective of regenerative medicine. Path-dependence, self-establishment and semi-autonomy of defined intermediate developmental stages might help in defining sufficient and necessary level of ex-vivo tissue growth to allow and guarantee further tissue maturation and integration upon implantation. Moreover, the combination with bioreactor based cell culture might facilitate the understanding and optimization of in vitro processes, towards the development of simplified and streamlined regenerative approaches.

Acknowledgements

The first acknowledgement goes to Prof Ueli Aebi and Prof Beppe Peretti for kindly accepting of being part of the PhD committee: I did appreciate your dedication, expertise and the great advice for my work.

Now it comes the time to thank Prof Ivan Martin: I realized one of my dreams working with you...thanks for being always so crystal clear. I am grateful for your mentoring, for work and life.

Many many many many thanks to Dr Andrea Barbero, precious, as always.

For Dr David Wendt, in line with your style..no words..just see you at cargo bar for a beer!